

High salt intake worsens aortic dissection in mice: involvement of IL-17A-dependent extracellular matrix metabolism

Norifumi Nishida, MD, Hiroki Aoki, MD, PhD *, Satoko Ohno-Urabe, MD, PhD, Michihide Nishihara, MD, PhD, Aya Furusho, MD, PhD, Saki Hirakata, MD, Makiko Hayashi, MD, Sohei Ito, MD, Hiroshi Yamada, PhD, Yuichiro Hirata, MD, PhD, Hideo Yasukawa, MD, PhD, Tsutomu Imaizumi, MD, PhD, Hiroyuki Tanaka, MD, PhD, Yoshihiro Fukumoto, MD, PhD

Running title: High salt, IL-17A, and worsening of aortic dissection

* Corresponding author

Cardiovascular Research Institute, Kurume University

67 Asahimachi, Kurume, Fukuoka 830-0011, Japan

phone; +81-942-31-7880

FAX; +81-942-31-7707

E-mail; haoki@med.kurume-u.ac.jp

Keywords: aortic dissection, IL-17, high salt, aortic wall stiffness

Subject terms: Animal Models of Human Disease, Aortic Dissection, Mechanisms

Total word count: 7,472

Total number of figures and tables: 11

TOC category: Basic study

TOC subcategory: Vascular Biology

ABSTRACT

Objective - Aortic dissection (AD) is a fatal disease that occurs suddenly without preceding clinical signs or symptoms. Although high salt intake is a proposed risk factor for cardiovascular diseases, the relationship between AD and high salt intake has not been clarified. We examined the effect of high salt challenge on a mouse AD model.

Approach and Results – AD was induced in male mice by continuous infusion of β -aminopropionitrile and angiotensin II. High salt challenge exacerbated aortic wall destruction in AD. Deletion of *Il17a* (IL-17KO) did not affect the AD phenotype at baseline, but it abolished the high salt-induced worsening of the aortic destruction. Unexpectedly, aortas of IL-17KO mice exhibited global changes in extracellular matrix-related genes without alteration of proinflammatory genes, altered architecture of collagen fibers, and reduced stiffness before AD induction. The aortas of IL-17KO mice were less sensitive to AD-inducing stimuli, as shown by the induction of phenotypic modulation markers SMemb and vimentin, suggesting a reduced stress response. The aortas of IL-17KO mice had a higher population of smooth muscle cells with nuclear-localized phospho-Smad2, indicative of TGF β signal activation. Consistently, pretreatment of smooth muscle cells in culture with IL-17A blunted the activation of Smad2 by TGF β 1.

Conclusions - These findings indicate that high salt intake has a worsening effect on AD in the context of high aortic wall stiffness, which is under the control of IL-17A through extracellular matrix metabolism. Therefore, salt restriction may represent a low-cost and practical way to reduce AD risk.

Non-standard Abbreviations and Acronyms

AD	aortic dissection
AngII	angiotensin II
BAPN	β -aminopropionitrile
BAV	bicuspid aortic valve
DAPI	4',6-diamidino-2-phenylindole
DAVID	Database for Annotation, Visualization, and Integrated Discovery
ECM	extracellular matrix
EVG	Elastica van Gieson
FBS	fetal bovine serum
HE	hematoxylin–eosin
IL	interleukin
KO	knock-out
N.S.	not significant
NF κ B	nuclear factor- κ B
PBS	phosphate-buffered saline
qRT-PCR	quantitative reverse transcription-polymerase chain reaction
SM2	smooth muscle myosin heavy chain
SMA	smooth muscle α -actin
SMC	smooth muscle cell
SMemb	embryonic isoform of myosin heavy chain
TAV	tricuspid aortic valves
WT	wild-type

INTRODUCTION

Aortic dissection (AD) is an abrupt tearing of the aortic wall, which is accompanied by severe pain and has largely unknown pathogenesis. AD is a serious medical emergency with high mortality, reaching 75% in 2 weeks without appropriate treatment because of rapid destruction of the aortic walls.¹ Despite recent advances in diagnostic modalities and surgical techniques, mortality associated with emergency surgery remains high (10% to 35%) at experienced centers. In addition to the high mortality of in-hospital patients, approximately 20% of patients die before reaching the hospital. No medical therapy is currently available to stabilize the injured aortic wall after AD develops. Though AD prevention is desirable, it is currently impractical because the condition has few, if any, warning signs before onset. In addition, because the annual incidence of AD in the general population is approximately 6 in 100,000,² medical intervention in the general population is considered impractical for preventing AD. Ambiguity about the pathogenesis of AD hampers the development of effective preventive and therapeutic interventions.

Recent studies using mouse models of AD have emphasized the importance of inflammatory molecules, including interleukin (IL)-6, granulocyte colony-stimulating factor, granulocyte-macrophage colony-stimulating factor, IL-17, Cxcl1, and Ccl2.³⁻⁶ We have also reported that tenascin C⁷ and myeloid cell Socs3,⁸ ameliorate AD by suppressing excessive proinflammatory responses and promoting adaptive metabolism in the extracellular matrix (ECM). However, how the inflammatory response and ECM metabolism are related in the context of AD pathogenesis remains unclear.

High salt intake is associated with a high incidence of cardiovascular disease, including hypertension,⁹ and aortic wall stiffening.¹⁰ Recent studies have demonstrated that high salt intake induces pathogenic Th17 cells, an IL-17-

producing cell type,^{11, 12} providing a link between high salt intake and inflammation. However, a link between high salt intake and AD has not been established.

In the current study, we explored the effect of high salt intake on AD development and the involvement of the IL-17 pathway. To investigate the molecular events preceding AD, we developed a new mouse model in which AD was induced by simultaneous infusion of angiotensin II (AngII) and β -aminopropionitrile (BAPN), a collagen/elastin crosslink inhibitor, for 14 days. As the AD developed in a quantitatively and chronologically predictable manner, this model allowed us to analyze the molecular events preceding AD development.

METHODS

The data, analytical methods, and study materials will be available to other researchers for the purpose of reproducing the results or replicating the procedure as long as the situation allows. For the sources of animals, cell lines, and antibodies, please see the Major Resources Table in the Supplemental Material. Expanded Methods are available in the Supplemental Material.

Animal experiments

All animal protocols were approved by the Animal Experiments Review Boards of Kurume University. All mice were fed normal chow and allowed access to freely available drinking water unless otherwise stated. All of the animal experiments were carried out using male mice aged 11-14 weeks because AD predominantly affects men.¹³ AD was induced by simultaneous administration of BAPN (150 mg/kg/day) and AngII (1000 ng/kg/min) using osmotic minipumps (Alzet model 1002). The mice were killed by pentobarbital overdose at the indicated time points (Supplemental Fig. S1) to obtain samples.

High salt challenge and genetic modification of mice

High salt challenge was achieved by substituting 1% NaCl for drinking water for the indicated time period. We used mice with a genetic deletion of *Il17a* (IL17-KO)¹⁴ to investigate the role of IL-17 in AD pathogenesis.

Quantitative assessment of AD lesions

The severity of AD is assessed by the extent and location of aortic wall destruction, which affects life-threatening complications, such as rupture, cardiac tamponade, and distal ischemia.^{15, 16} Three-dimensional analysis of our mouse AD model indicated progressive disruption of multiple medial layers associated with the formation of intramural hematoma and increased aortic diameter.¹⁷ Accordingly,

the lesions with aortic wall destruction due to AD were defined in this study by a diameter at least 1.5-fold greater than the reference diameter (Supplemental Fig. S2). The aortic rupture rate was also assessed.

Expression analysis

Immunoblotting was performed with antibodies as indicated in the Major Resources Table. Plasma levels of IL-17A were measured using a bead-based assay (Bio-Plex, Bio-Rad #171-G5013M). We performed transcriptome analyses using the SurePrint G3 Mouse Gene Expression v2 8x60K Microarray Kit (Agilent). The dataset has been deposited to the Gene Expression Omnibus of the National Center for Biotechnology Information (accession # GSE116434). Gene enrichment analysis was performed using the Database for Annotation, Visualization, and Integrated Discovery (DAVID, <https://david.ncicrf.gov/>).¹⁸ Expression of the indicated genes were measured by quantitative reverse transcription-polymerase chain reaction (qRT-PCR) using commercially available probes (Qiagen).

Histological analysis

We performed Elastica van Gieson (EVG) or hematoxylin–eosin (HE) staining on 5- μ m sections. Imaging cytometric analysis of mouse aortas was performed using ArrayScan XTI (Thermo Fisher Scientific) and FlowJo 10 software (FlowJo). Two aortic tissue sections were obtained from each mouse in the WT (n=8) and IL-17KO (n=8) groups, stained as indicated in the Major Resources Table.

Collagen deposition in aortic walls

For the histological analysis of collagen deposition, we stained the aortic tissue sections with picrosirius red. Bright field and polarized light-illuminated histological images were used. The collagen deposition area were measured using ImagePro Plus software (version 7.0.1, Media Cybernetics).

Stiffness of the aortic walls

To measure the mechanical properties of the aorta, we used a device that we developed (Muromachi Kikai, Japan, Supplemental Fig. S3). The aortic ring was immersed in calcium-free PBS containing 10 mM 2,3-butanedione monoxim to suppress smooth muscle cell (SMC) contraction. As an index of aortic wall stiffness, we calculated the mean force/displacement ratio from 0 mN to 5 mN, which corresponds to approximately 0 mmHg to 80 mmHg of blood pressure.

Cell culture experiments

Mouse aortic SMCs (#JCRB0150) were maintained in Dulbecco's modified Eagle's medium (DMEM) with high glucose and fetal bovine serum (FBS). Serum-starved SMCs were stimulated with or without 25 ng/mL recombinant mouse IL-17A (R&D Systems, Minneapolis, MN, USA) for 24 hours, followed by 10 ng/mL recombinant mouse TGF β 1 (R&D Systems) for 1 hour.

Data acquisition and statistical analysis

Animals were randomly assigned to the experimental groups. The data were acquired by researchers or technicians who were blinded to the genetic modification and experimental intervention of the mice. All data are expressed as means \pm standard errors. Statistical analyses were performed with GraphPad PRISM 5 (GraphPad Software). Significance was indicated by a two-sided $p < 0.05$.

RESULTS

Mouse model of AD

In this study, we intended to analyze the molecular changes preceding AD development and during aortic wall destruction after AD development. We modified a previously reported AD model¹⁹ to induce more gradual changes. We simultaneously infused BAPN and AngII using osmotic minipumps, which allowed us to examine the time course of molecular and pathological changes from normal aorta to AD over 14 days of BAPN+AngII administration (Fig. 1). Histological analysis of AD in this model revealed disruption of the tunica media with intramural hematoma, a hallmark of human AD, and infiltration of inflammatory cells mainly in the tunica adventitia. The incidence of AD and aortic wall lesions due to AD increased with BAPN dose (Fig. 1B), and we deliberately chose 150 mg/kg/day BAPN, which caused AD in approximately 90% of mice and aortic rupture in approximately 30% of mice, allowing the detection of either a better or worse outcome. Three dimensional analysis of this model revealed progressive destruction of the aortic walls compatible with AD.¹⁷ Transcriptome analysis 3 days after starting BAPN+AngII, but before the onset of AD, revealed the induction of 1,722 (6.03%) probes and the suppression of 1,207 (4.23%) probes among the 28,562 probes with reliable signals (Fig. 1C). To test the relevance of this mouse AD model to human AD, we performed annotation analysis for the previously reported transcriptome for aortas with congenital bicuspid aortic valve (BAV),²⁰ as patients with BAV are prone to AD. The BAV aorta exhibited significant induction of 366 (1.58%) genes and the suppression of 477 (1.22%) genes among 30,121 probes with reliable signals compared to aortic samples with normal tricuspid aortic valves (TAVs) (Fig. 1C). We analyzed the functional annotation of these datasets using DAVID (Supplemental Tables S1 and S2).¹⁸ Our BAPN+AngII model shared common gene annotations with BAV: cell proliferation, cell migration, morphogenesis, and smooth muscle regulation (Table 1). These gene expression

profiles in AD model were also consistent with those observed in human AD,²¹ indicating that this model shares various aspects of human AD. In addition, BAPN+AngII caused an inflammatory response, which is likely to contribute to the rapid development of AD in this model.¹⁹

Effect of high salt challenge on AD and the involvement of IL-17

We tested the effect of high salt intake by giving AD mice 1% NaCl as drinking water 1 week prior to and during the BAPN+AngII infusion and made comparisons with the normal salt-intake group. The high salt challenge did not affect the systolic blood pressure or pulse rate of the mice (Supplemental Fig. S4). The length of aortic wall destruction due to AD was significantly greater in the aortic arch, descending thoracic, and total aorta in the high salt group compared to the normal salt group (Figs. 2A and 2B, Supplemental Fig. S5). Recent studies have proposed that high salt intake activates IL-17 via the induction of pathogenic Th17 cells.^{11, 12} In the normal salt condition, the length of aortic wall destruction was comparable between WT and IL-17KO mice. However, the worsening of AD by high salt challenge was abolished in IL-17KO mice (Figs. 2A, 2B, Supplemental Fig. S5). The aortic rupture was also increased by high salt challenge only in WT mice (Table 2). These findings indicate that the worsening effect of high salt on AD was dependent on IL-17A.

To examine whether high salt challenge activated the IL-17 pathway, we examined the plasma concentration of IL-17A and mRNA expression of *Il17a* in the aortic tissue (Fig. 2C). However, neither high salt nor BAPN+AngII induced the expression of IL-17A. Next, we examined the mRNA expression levels of *Rorc*, a marker of Th17, and *Tcrg*, a marker of $\gamma\delta$ T cells, and the IL-17A cognate receptor genes *Il-17ra* and *Il-17rc* in the mouse aorta (Fig. 2D). High salt challenge showed no effect and BAPN+AngII suppressed these markers in IL-17-producing cell types. High salt challenge induced IL-17 receptors, but BAPN+AngII suppressed

this expression. These findings indicate that high salt or BAPN+AngII challenge did not induce IL-17-producing cells in the aortic tissue or increase the plasma IL-17A concentration, but it modulated the gene expression of IL-17 receptors.

Effect of high salt challenge on IL-17 downstream signaling and transcriptome

We examined whether the modulation of the expression of IL-17 receptors by high salt challenge resulted in activation of the NFκB pathway, canonical downstream signaling in the IL-17 pathway. High salt challenge for 10 days did not result in changes to the expression of total or phosphorylated (activated) NFκB in the aorta (Fig. 3A). In the transcriptome analyses, high salt challenge caused changes in the expression of only 0.5% of the detected genes with or without 3 days of BAPN+AngII or *Il-17a* deletion (Fig. 3B). Considering that BAPN+AngII, an AD-inducing stimuli, resulted in changes in the expression of approximately 10% of the genes (Fig. 1C), it was unlikely that high salt challenge caused fundamental changes in the aortic tissue response to the AD-inducing stimuli. The annotation analysis for the high salt-sensitive genes revealed only weak enrichment of xenobiotic metabolism (enrichment score 2.04, Table 3), which may not have direct involvement in AD pathogenesis or IL-17 signaling. Therefore, although high salt challenge exacerbated AD in an IL-17A-dependent manner and modulated the expression of IL-17 receptors, it was unlikely to have a direct effect on the downstream signaling or aortic tissue response in the IL-17 pathway.

Impact of *Il17a* gene deletion on the aorta gene expression profile

We examined whether *Il17a* deletion has an impact on the aortic tissue in the transcriptome analysis. Unexpectedly, *Il17a* deletion alone resulted in changes to the expression of 14.0% of the detected genes (Fig. 4A). We performed the gene annotation analysis for the differentially expressed genes (Table 3) and revealed

enrichment of morphogenesis-related genes in the aortas of IL-17KO mice (Table 3), suggesting that IL-17A plays a role in maintaining tissue architecture. As ECM is essential for the aortic tissue architecture and abnormalities in the ECM participate in AD pathogenesis, we assessed 550 genes with Gene Ontology terms that include “extracellular matrix”. As indicated by the heatmap of the hierarchical clustering analysis (Fig. 4B, Supplemental Table S3), aorta from IL-17KO mice exhibited differential expression of 237 out of 550 ECM-related genes compared to aortas from WT mice at baseline. These findings suggest that IL-17A may be involved in ECM metabolism.

Involvement of IL-17A in ECM metabolism

To further investigate the impact of IL-17A on ECM metabolism before AD induction, we examined collagen fibers in the aorta using picrosirius red stain (Figs. 5A and 5B). The aortic media in IL-17 KO mice had higher collagen content than WT mice, regardless of the high salt challenge. The observation of picrosirius red-stained aorta with polarized illumination revealed bright yellow to red color, indicative of the mature collagen in the adventitia of the aortas of WT mice (Figs. 5C and 5D). Mature collagen was less abundant in the adventitia and more abundant in the media of IL-17KO mice. In contrast to collagen fibers, elastin fibers as detected by EVG staining were not different between WT and IL-17KO aortas (Figs. 5E and 5F). These findings underscore the importance of IL-17 in ECM metabolism, especially of collagen fibers in the aorta.

We examined the mechanical properties of aortic rings excised from the descending aortas of WT and IL-17KO mice. We measured the passive force-displacement relationship as an index of the aortic wall stiffness and the peak force when the aortic rings broke (Figs. 5G and 5H, Supplemental Fig. S3). The individual and averaged force-displacement curves of IL-17KO samples had a rightward shift compared to WT samples (Fig. 5G). We calculated the mean

force/displacement ratio from 0 mN to 5 mN, which approximately corresponds to 0 mmHg to 80 mmHg of blood pressure. The mean force/displacement ratio was significantly lower in the aortas of IL-17KO mice compared to WT mice (Fig. 5H). On the other hand, the peak force development, corresponding to the aortic ring breakage, did not differ between WT and IL-17KO mice. Therefore, the stiffness of aortas was significantly lower in IL-17KO mice than WT mice (0 mmHg - 80 mmHg), but the ultimate tensile strength in the aorta did not differ between WT and IL-17KO mice.

Effect of IL-17 gene deletion on TGF β signaling in the aorta

Next, we examined the Smad pathway, which plays a central role in ECM metabolism (Figs. 6A and 6B). P-Smad2 or P-Smad3 did not show statistically significant difference among the experimental groups. As for Smad7, an inhibitory Smad, IL-17KO mice had significantly lower expression of Smad7 compared to WT animals in high salt condition. Expression of total Smad2 or Smad3 did not change with high salt challenge or in IL-17KO. In contrast, expression of Smad4 was significantly higher in IL-17KO aorta regardless of the high salt challenge.

To understand Smad signaling at the single cell level, we performed immunofluorescent staining and imaging cytometry for nuclear P-Smad2 and SMA, a marker of SMCs (Figs. 6C and 6D, Supplemental Figs. S7 and S8). The cell population with nuclear P-Smad2 was 49.2% for aortas from WT mice and 55.1% for aortas from IL-17KO mice. For SMA-negative non-SMCs, the P-Smad2-positive cell population was comparable between WT (41.9%) and IL-17KO (43.1%) mice, whereas for SMA-positive SMCs, the P-Smad2-positive cell population was higher in IL-17KO (45.9%) than in WT (36.1%) mice. These findings suggest that IL-17A interferes with Smad signaling in SMCs.

Crosstalk of IL-17 and TGF β pathways in aortic smooth muscle cells

We examined the crosstalk between the IL-17A and TGF β pathways in aortic SMCs in culture (Fig. 7). Administration of IL-17A resulted in the transient activation of Jnk, indicating that SMCs were responsive to exogenous IL-17A. Administration of TGF β 1 caused prominent phosphorylation of both Smad2 and Smad3 in SMCs. Pretreatment of aortic SMCs with IL-17A for 24 hours resulted in no significant change in the phosphorylation of Smad2 or Smad3. However, IL-17A pretreatment significantly suppressed the subsequent activation of Smad2 and Smad3 by TGF β 1. Administration of IL-17A or TGF β 1 caused no significant changes in the expression of Smad2, Smad3, or Smad4. These findings demonstrate the suppressive effect of IL-17A on TGF β signaling in aortic SMCs.

Phenotypic modulation of SMCs and the inflammatory response in the aorta

Vascular SMCs change their phenotype in response to various stress stimuli for homeostasis, adaptation, and tissue remodeling.²² Accordingly, we examined the expression of SMC phenotype markers SMemb and vimentin as synthetic phenotype markers, and SM2 and calponin-1 as contractile phenotype markers (Fig. 8). In WT mice, expression of SMemb tended to increase with high salt challenge, BAPN+AngII challenge, or both, and the induction was significant only with both challenges. In IL-17KO mice, the increase in SMemb expression upon high salt and BAPN+AngII challenge was less significant compared to WT mice. SMemb expression was higher in IL-17KO aorta than in WT aorta at baseline. Expression of vimentin also increased with high salt and BAPN+AngII challenge in WT mice ($p < 0.01$, ANOVA), but not IL-17KO mice ($p = 0.71$, ANOVA). Expression of SM2 and calponin-1 did not significantly change with high salt or BAPN+AngII challenge or between WT and IL-17KO mice.

We also examined the activation (phosphorylation) of Stat3 and Jnk, important signal mediators for aortopathies (Fig. 9).^{3-6, 19, 23} High salt challenge alone caused no significant changes, whereas BAPN+AngII caused a slight increase in P-Stat3

or P-Jnk. Combination of high salt and BAPN+AngII challenge caused a significant increase in P-Stat3 in both WT and IL-17KO mice. As for P-Jnk, BAPN+AngII and high salt challenges caused significant increase in WT aorta, but not in IL17-KO aorta. These findings suggest that, while combination of BAPN+AngII and high salt challenges exaggerated proinflammatory response as shown by P-Stat3 and P-Jnk in the aorta, deletion of *Il17a* rendered the aorta less sensitive to the challenges in terms of the phenotypic modulation of SMCs.

DISCUSSION

In this study, we demonstrated that high salt challenge worsened AD, which was dependent on the presence of IL-17A. Unexpectedly, deletion of *Il17a* resulted in less aorta stiffness, which was associated with a lesser stress response as assessed by phenotypic markers of SMCs without detectable changes in the inflammatory response in our experimental condition. High salt challenge did not seem to alter the gross aortic response as assessed by transcriptome analysis. However, high salt challenge augmented the BAPN+AngII-induced activation of Jnk and Stat3 and phenotypic changes in SMCs, suggesting an enhanced stress on the aortic wall.

IL-17 plays a critical role in acute inflammation²⁴ and is reported to participate in AD pathogenesis by promoting inflammation.⁴ However, *Il17a* deletion did not alter the inflammatory response 3 days after BAPN+AngII challenge in our AD model. This could be due to differences in the AD models; we induced AD by BAPN+AngII infusion in young mice, whereas Brasier *et al.* used AngII infusion alone in aged mice,^{3, 4} which may express higher levels of IL-17.^{25, 26} Another possibility is that, IL-17A may participate in inflammation in later stages of AD. Instead of regulating inflammation, the data indicated that IL-17A regulates nearly half of the 550 ECM-related genes. Although IL-17A has been reported to regulate matrix metalloproteinases in the context of inflammation,²⁷⁻²⁹ this is the first report that IL-17A participates in global ECM metabolism in normal physiology without obvious inflammation.

Another novel finding in this study is the crosstalk between the IL-17 and TGF β pathways. Pretreatment of cultured SMCs with IL-17A resulted in a blunted response of Smad2 and Smad3 activation by TGF β 1. In the chronic in vivo situation without IL-17A, nuclear localization of P-Smad2 was observed preferentially in SMCs. The nuclear localization of P-Smad2 may be explained by the altered expression of Smad4 that is essential for nuclear localization of

Smad2/3.³⁰ Alternatively, the TGF β signaling may undergo direct interference by IL-17A, as observed in the cell culture experiments. Because TGF β is a main regulator of ECM metabolism and SMC differentiation,³¹ altered TGF β signaling may explain such changes in the ECM metabolism of IL-17KO aortas.

The global changes in gene expression and altered architecture of ECM are likely the basis for the reduced stiffness of the aortic wall in IL-17KO mice. Aortic stiffness is a risk factor for cardiovascular events³² and is associated with genetic and non-genetic aortopathies, including AD, in humans.³³ In patients with Marfan syndrome, the stiffness predicts aortic dilation.³⁴ Aortic stiffness is increased in the mouse Marfan model,³⁵ and the increase in aortic stiffness is associated with increased propensity for AD.⁷ In this regard, it is noteworthy that the beneficial effect of *Il17a* deletion was observed only in mice with high salt challenge, a situation in which augmented hemodynamic stress has been reported due to an increase in plasma volume.¹⁰

High salt intake is proposed to be a risk factor for cardiovascular diseases, including hypertension,³⁶ a risk factor for AD.³⁷ However, whether high salt intake is truly a risk factor for cardiovascular diseases is unclear.³⁸ In addition, high salt intake has not been demonstrated to be a risk factor for AD. This could be due to the confounding factors and variability in individual physiology.³⁸ In this regard, it is of interest that high salt intake promoted the AD model only in WT mice in this study, but not in IL-17KO mice, in which ECM metabolism and aortic stiffness are different. This finding can be interpreted as high salt intake being a risk factor for AD is dependent on the physiological conditions of the aorta, such as wall stiffness.

Taken together, our findings indicate that high salt intake worsened AD only in the presence of intact IL-17A expression. IL17A plays a pivotal role in aortic wall homeostasis, possibly by modulating TGF β signaling and ECM metabolism, resulting in stiffening of the aorta (Supplemental Fig. S9). Further studies are

required for risk stratification and management for AD predisposition, taking aortic wall stiffness and high salt intake into account.

Acknowledgments

We would like to thank Ms. Kiyohiro, Mr. Watanabe, Mr. Yo, Mr. Koga, Mr. Inuzuka, Ms. Nishigata, Ms. Nakao, Ms. Shiramizu, Ms. Nakayama, and Dr. Yamamoto for their technical assistance.

Sources of Funding

This work was funded in part by grants from Japan Society for the Promotion of Science (25861236 and 16K19973 to N.N.; 21390367, 24390334, 24659640, 26670621, and 16H05428 to H.A.); Daiichi Sankyo Foundation of Life Science, the Uehara Memorial Foundation (to H.A.), the Vehicle Racing Commemorative Foundation (to H.A.), Bristol-Myers Squibb (to H.A.); and TaNeDS grants from Daiichi Sankyo (to H.A.).

Disclosures

None

Affiliations

Division of Cardiovascular Medicine, Department of Internal Medicine, Kurume University School of Medicine, Kurume, Japan (N.N., S.O.-U., M.N., A.F., S.H., M.H., S.I., H.Yas., Y.F.); Cardiovascular Research Institute, Kurume University, Kurume, Japan (H.A.); Department of Biological Functions Engineering, Graduate School of Life Science and Systems Engineering, Kyushu Institute of Technology, Kitakyushu, Japan (H.Yam.); Division of Cardiovascular Surgery, Department of Surgery, Kurume University School of Medicine, Kurume, Japan (Y.H., H.T.); International University of Health and Welfare, Fukuoka, Japan (T.I.).

References

1. Crawford ES. The diagnosis and management of aortic dissection. *JAMA*. 1990;264:2537-2541
2. Nienaber CA, Clough RE. Management of acute aortic dissection. *Lancet*. 2015;385:800-811
3. Tieu BC, Lee C, Sun H, Lejeune W, Recinos A, 3rd, Ju X, Spratt H, Guo DC, Milewicz D, Tilton RG, Brasier AR. An adventitial IL-6/MCP1 amplification loop accelerates macrophage-mediated vascular inflammation leading to aortic dissection in mice. *J Clin Invest*. 2009;119:3637-3651
4. Ju X, Ijaz T, Sun H, Ray S, Lejeune W, Lee C, Recinos A, 3rd, Guo DC, Milewicz DM, Tilton RG, Brasier AR. Interleukin-6-signal transducer and activator of transcription-3 signaling mediates aortic dissections induced by angiotensin II via the T-helper lymphocyte 17-interleukin 17 axis in C57BL/6 mice. *Arterioscler Thromb Vasc Biol*. 2013;33:1612-1621
5. Anzai A, Shimoda M, Endo J, Kohno T, Katsumata Y, Matsushashi T, Yamamoto T, Ito K, Yan X, Shirakawa K, Shimizu-Hirota R, Yamada Y, Ueha S, Shinmura K, Okada Y, Fukuda K, Sano M. Adventitial CXCL1/G-CSF expression in response to acute aortic dissection triggers local neutrophil recruitment and activation leading to aortic rupture. *Circ Res*. 2015;116:612-623
6. Son BK, Sawaki D, Tomida S, Fujita D, Aizawa K, Aoki H, Akishita M, Manabe I, Komuro I, Friedman SL, Nagai R, Suzuki T. Granulocyte macrophage colony-stimulating factor is required for aortic dissection/intramural haematoma. *Nat Commun*. 2015;6:6994
7. Kimura T, Shiraishi K, Furusho A, Ito S, Hirakata S, Nishida N, Yoshimura K, Imanaka-Yoshida K, Yoshida T, Ikeda Y, Miyamoto T, Ueno T, Hamano K, Hiroe M, Aonuma K, Matsuzaki M, Imaizumi T, Aoki H. Tenascin C protects aorta from acute dissection in mice. *Sci Rep*. 2014;4:4051

8. Ohno-Urabe S, Aoki H, Nishihara M, Furusho A, Hirakata S, Nishida N, Ito S, Hayashi M, Yasukawa H, Imaizumi T, Akashi H, Tanaka N, Fukumoto Y. The role of macrophage Socs3 in the pathogenesis of aortic dissection. 2017
9. Strazzullo P, D'Elia L, Kandala NB, Cappuccio FP. Salt intake, stroke, and cardiovascular disease: meta-analysis of prospective studies. *BMJ*. 2009;339:b4567
10. Cordaillat M, Reboul C, Gaillard V, Lartaud I, Jover B, Rugale C. Plasma volume and arterial stiffness in the cardiac alterations associated with long-term high sodium feeding in rats. *Am J Hypertens*. 2011;24:451-457
11. Kleinewietfeld M, Manzel A, Titze J, Kvakana H, Yosef N, Linker RA, Muller DN, Hafler DA. Sodium chloride drives autoimmune disease by the induction of pathogenic TH17 cells. *Nature*. 2013;496:518-522
12. Wu C, Yosef N, Thalhamer T, Zhu C, Xiao S, Kishi Y, Regev A, Kuchroo VK. Induction of pathogenic TH17 cells by inducible salt-sensing kinase SGK1. *Nature*. 2013;496:513-517
13. Nienaber CA, Fattori R, Mehta RH, Richartz BM, Evangelista A, Petzsch M, Cooper JV, Januzzi JL, Ince H, Sechtem U, Bossone E, Fang J, Smith DE, Isselbacher EM, Pape LA, Eagle KA, International Registry of Acute Aortic D. Gender-related differences in acute aortic dissection. *Circulation*. 2004;109:3014-3021
14. Ishigame H, Kakuta S, Nagai T, Kadoki M, Nambu A, Komiyama Y, Fujikado N, Tanahashi Y, Akitsu A, Kotaki H, Sudo K, Nakae S, Sasakawa C, Iwakura Y. Differential roles of interleukin-17A and -17F in host defense against mucosal bacterial infection and allergic responses. *Immunity*. 2009;30:108-119
15. Hiratzka LF, Bakris GL, Beckman JA, Bersin RM, Carr VF, Casey DE, Jr., Eagle KA, Hermann LK, Isselbacher EM, Kazerooni EA, Kouchoukos NT,

- Lytle BW, Milewicz DM, Reich DL, Sen S, Shinn JA, Svensson LG, Williams DM, American College of Cardiology Foundation/American Heart Association Task Force on Practice G, American Association for Thoracic S, American College of R, American Stroke A, Society of Cardiovascular A, Society for Cardiovascular A, Interventions, Society of Interventional R, Society of Thoracic S, Society for Vascular M. 2010 ACCF/AHA/AATS/ACR/ASA/SCA/SCAI/SIR/STS/SVM Guidelines for the diagnosis and management of patients with thoracic aortic disease. *J Am Coll Cardiol.* 2010;55:e27-e129
16. Cronenwett JL, Johnston KW. *Vascular Surgery*. Philadelphia: Elsevier Health Sciences; 2014.
 17. Logghe G, Trachet B, Aslanidou L, Villaneuva-Perez P, De Backer J, Stergiopoulos N, Stampanoni M, Aoki H, Segers P. Propagation-based phase-contrast synchrotron imaging of aortic dissection in mice: from individual elastic lamella to 3D analysis. *Sci Rep.* 2018;8:2223
 18. Huang da W, Sherman BT, Lempicki RA. Systematic and integrative analysis of large gene lists using DAVID bioinformatics resources. *Nat Protoc.* 2009;4:44-57
 19. Kurihara T, Shimizu-Hirota R, Shimoda M, Adachi T, Shimizu H, Weiss SJ, Itoh H, Hori S, Aikawa N, Okada Y. Neutrophil-derived matrix metalloproteinase 9 triggers acute aortic dissection. *Circulation.* 2012;126:3070-3080
 20. Hirata Y, Aoki H, Shojima T, Takagi K, Takaseya T, Akasu K, Tobinaga S, Fukumoto Y, Tanaka H. Activation of the AKT Pathway in the Ascending Aorta With Bicuspid Aortic Valve. *Circ J.* 2018;82:2485-2492
 21. Muller BT, Modlich O, Prisack HB, Bojar H, Schipke JD, Goecke T, Feindt P, Petzold T, Gams E, Muller W, Hort W, Sandmann W. Gene expression

- profiles in the acutely dissected human aorta. *Eur J Vasc Endovasc Surg.* 2002;24:356-364
22. Frismantiene A, Philippova M, Erne P, Resink TJ. Smooth muscle cell-driven vascular diseases and molecular mechanisms of VSMC plasticity. *Cell Signal.* 2018;52:48-64
 23. Yoshimura K, Aoki H, Ikeda Y, Fujii K, Akiyama N, Furutani A, Hoshii Y, Tanaka N, Ricci R, Ishihara T, Esato K, Hamano K, Matsuzaki M. Regression of abdominal aortic aneurysm by inhibition of c-Jun N-terminal kinase. *Nat Med.* 2005;11:1330-1338
 24. von Vietinghoff S, Ley K. Interleukin 17 in vascular inflammation. *Cytokine Growth Factor Rev.* 2010;21:463-469
 25. Kang JY, Lee SY, Rhee CK, Kim SJ, Kwon SS, Kim YK. Effect of aging on airway remodeling and muscarinic receptors in a murine acute asthma model. *Clin Interv Aging.* 2013;8:1393-1403
 26. De Angulo A, Faris R, Cavazos D, Jolly C, Daniel B, DeGraffenried L. Age-related alterations in T-lymphocytes modulate key pathways in prostate tumorigenesis. *Prostate.* 2013;73:855-864
 27. Camargo LDN, Righetti RF, Aristoteles L, Dos Santos TM, de Souza FCR, Fukuzaki S, Cruz MM, Alonso-Vale MIC, Saraiva-Romanholo BM, Prado CM, Martins MA, Leick EA, Tiberio I. Effects of Anti-IL-17 on Inflammation, Remodeling, and Oxidative Stress in an Experimental Model of Asthma Exacerbated by LPS. *Front Immunol.* 2017;8:1835
 28. Nakashima T, Jinnin M, Yamane K, Honda N, Kajihara I, Makino T, Masuguchi S, Fukushima S, Okamoto Y, Hasegawa M, Fujimoto M, Ihn H. Impaired IL-17 signaling pathway contributes to the increased collagen expression in scleroderma fibroblasts. *J Immunol.* 2012;188:3573-3583
 29. Chakir J, Shannon J, Molet S, Fukakusa M, Elias J, Laviolette M, Boulet LP, Hamid Q. Airway remodeling-associated mediators in moderate to severe

- asthma: effect of steroids on TGF-beta, IL-11, IL-17, and type I and type III collagen expression. *J Allergy Clin Immunol.* 2003;111:1293-1298
30. Watanabe M, Masuyama N, Fukuda M, Nishida E. Regulation of intracellular dynamics of Smad4 by its leucine-rich nuclear export signal. *EMBO Rep.* 2000;1:176-182
 31. MacFarlane EG, Haupt J, Dietz HC, Shore EM. TGF-beta Family Signaling in Connective Tissue and Skeletal Diseases. *Cold Spring Harb Perspect Biol.* 2017
 32. Cavalcante JL, Lima JA, Redheuil A, Al-Mallah MH. Aortic stiffness: current understanding and future directions. *J Am Coll Cardiol.* 2011;57:1511-1522
 33. Grillo A, Pini A, Marelli S, Gan L, Giuliano A, Trifiro G, Santini F, Salvi L, Salvi P, Viecca F, Carretta R, Parati G. 5b.05: Marfan Syndrome: Assessment of Aortic Dissection Risk by Analysis of Aortic Viscoelastic Properties. *J Hypertens.* 2015;33 Suppl 1:e67
 34. Nollen GJ, Groenink M, Tijssen JG, Van Der Wall EE, Mulder BJ. Aortic stiffness and diameter predict progressive aortic dilatation in patients with Marfan syndrome. *Eur Heart J.* 2004;25:1146-1152
 35. Marque V, Kieffer P, Gayraud B, Lartaud-Idjouadiene I, Ramirez F, Atkinson J. Aortic wall mechanics and composition in a transgenic mouse model of Marfan syndrome. *Arterioscler Thromb Vasc Biol.* 2001;21:1184-1189
 36. Whelton PK. Sodium, blood pressure, and cardiovascular disease: a compelling scientific case for improving the health of the public. *Circulation.* 2014;129:1085-1087
 37. LeMaire SA, Russell L. Epidemiology of thoracic aortic dissection. *Nat Rev Cardiol.* 2011;8:103-113
 38. O'Donnell MJ, Mente A, Smyth A, Yusuf S. Salt intake and cardiovascular disease: why are the data inconsistent? *Eur Heart J.* 2013;34:1034-1040

Highlights

- Aortic dissection (AD) is a sudden, unpredictable and fatal aortic destruction of which disease mechanism is largely unknown.
- IL-17A interfered with TGF β signal, altered extracellular matrix metabolism, and made aortic walls stiffer.
- High salt challenge exacerbated aortic wall destruction in AD only when IL-17A was intact and aortic wall was stiff.
- Salt restriction may represent a low-cost and practical way to reduce AD risk for those who have stiffened aortic walls.

BAPN+AngII vs. Control

Enrichment Score: 17.16

GO:0008283~cell proliferation
GO:0042127~regulation of cell proliferation
GO:0008284~positive regulation of cell proliferation

Enrichment Score: 13.92

GO:1903047~mitotic cell cycle process
GO:0000278~mitotic cell cycle
GO:0007049~cell cycle

Enrichment Score: 11.89

GO:0006954~inflammatory response
GO:0032101~regulation of response to external stimulus
GO:0006952~defense response

Enrichment Score: 10.66

GO:0006955~immune response
GO:0006952~defense response
GO:0045087~innate immune response

Enrichment Score: 9.92

GO:0050900~leukocyte migration
GO:0060326~cell chemotaxis
GO:0030595~leukocyte chemotaxis

Enrichment Score: 9.24

GO:0001775~cell activation
GO:0045321~leukocyte activation
GO:0016337~single organismal cell-cell adhesion

Enrichment Score: 8.39

GO:0032103~positive regulation of response to external stimulus
GO:0050727~regulation of inflammatory response
GO:0031349~positive regulation of defense response

Enrichment Score: 8.32

GO:1903047~mitotic cell cycle process
GO:0000278~mitotic cell cycle
GO:0022402~cell cycle process

Enrichment Score: 7.51

GO:0023051~regulation of signaling
GO:0010646~regulation of cell communication
GO:0009966~regulation of signal transduction

Enrichment Score: 7.29

GO:0006259~DNA metabolic process
GO:0006974~cellular response to DNA damage stimulus
GO:0006281~DNA repair

Enrichment Score: 5.33

GO:0051240~positive regulation of multicellular organismal process
GO:2000026~regulation of multicellular organismal development
GO:0051094~positive regulation of developmental process

Enrichment Score: 2.13

GO:0008015~blood circulation
GO:0006939~smooth muscle contraction
GO:0042311~vasodilation

BAV vs. TAV

Enrichment Score: 2.23

GO:0030335~positive regulation of cell migration
GO:0030334~regulation of cell migration
GO:2000145~regulation of cell motility

Enrichment Score: 2.15

GO:0090505~epiboly involved in wound healing
GO:0044319~wound healing, spreading of cells
GO:0090504~epiboly

Enrichment Score: 2.10

GO:0022607~cellular component assembly
GO:0044085~cellular component biogenesis
GO:0043933~macromolecular complex subunit organization

Enrichment Score: 2.09

GO:0010927~cellular component assembly involved in morphogenesis
GO:0030031~cell projection assembly
GO:0042384~cilium assembly

Enrichment Score: 1.94

GO:0008283~cell proliferation
GO:0008284~positive regulation of cell proliferation
GO:0042127~regulation of cell proliferation

Enrichment Score: 1.78

GO:0051276~chromosome organization
GO:0016569~covalent chromatin modification
GO:0016570~histone modification

Enrichment Score: 1.69

GO:0051150~regulation of smooth muscle cell differentiation
GO:0051151~negative regulation of smooth muscle cell differentiation
GO:0051145~smooth muscle cell differentiation

Enrichment Score: 1.67

GO:0007265~Ras protein signal transduction
GO:0007264~small GTPase mediated signal transduction
GO:0046578~regulation of Ras protein signal transduction

Table 1. Enrichment analysis of GO terms in transcriptomes of the mouse AD model and human BAV aorta.

Biological process (BP)-focused gene ontology (GO) enrichment analysis was performed for the differentially expressed genes in the transcriptome of the mouse AD model compared to normal aorta (left column), and human BAV aorta compared to TAV aorta (right column). The GO terms are color-coded for those related to cell proliferation (blue), cell migration (cyan), cell and tissue morphogenesis (red), and smooth muscle regulation (green).

Genotype /Salt	WT /Normal	WT /High	IL-17KO /Normal	IL-17KO /High
No rupture	14 (87.5%)	9 (56.3%)	14 (87.5%)	13 (81.3%)
Total rupture	2 (12.5%)	7 (43.8%)	2 (12.5%)	3 (18.8%)
Thoracic	2 (12.5%)	3 (18.8%)	0 (0.0%)	2 (12.5%)
Abdominal	0 (0.0%)	4 (25.0%)	2 (12.5%)	1 (6.3%)
Total	16 (100.0%)	16 (100.0%)	16 (100.0%)	16 (100.0%)

Table 2. Effect of high salt on fatal aortic rupture.

The numbers of aortic rupture are shown, of which location was either thoracic or abdominal aorta. Percentages in a given group are shown in parentheses. Chi-square test revealed significant difference between normal and high salt groups for the total rupture number in wild type mice (WT, $p < 0.05$), whereas no significant difference was observed in IL-17KO mice.

Na_change_GO_BP_FAT

Enrichment Score: 2.04

GO:0017144~drug metabolic process
GO:0006805~xenobiotic metabolic process
GO:0071466~cellular response to xenobiotic stimulus

IL-17-KO_change_GO_BP_FAT

Enrichment Score: 5.72

GO:0010646~regulation of cell communication
GO:0023051~regulation of signaling
GO:0009966~regulation of signal transduction

Enrichment Score: 5.10

GO:0001763~morphogenesis of a branching structure
GO:0002009~morphogenesis of an epithelium
GO:0060429~epithelium development

Enrichment Score: 4.80

GO:0009887~organ morphogenesis
GO:0090596~sensory organ morphogenesis
GO:0007389~pattern specification process

Enrichment Score: 4.17

GO:0001763~morphogenesis of a branching structure
GO:0072001~renal system development
GO:0072073~kidney epithelium development

Enrichment Score: 4.03

GO:0007267~cell-cell signaling
GO:0098916~anterograde trans-synaptic signaling
GO:0007268~chemical synaptic transmission

Enrichment Score: 3.901

GO:0007399~nervous system development
GO:0048468~cell development
GO:0006935~chemotaxis

Enrichment Score: 3.83

GO:0042063~gliogenesis
GO:0010001~glial cell differentiation
GO:0014013~regulation of gliogenesis

Enrichment Score: 3.81

GO:0044708~single-organism behavior
GO:0007626~locomotory behavior
GO:0007610~behavior

Enrichment Score: 3.74

GO:0048514~blood vessel morphogenesis
GO:0072359~circulatory system development
GO:0001525~angiogenesis

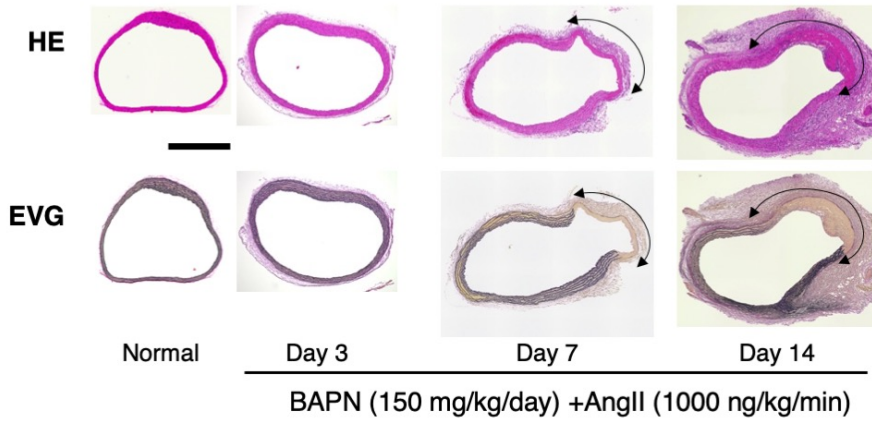
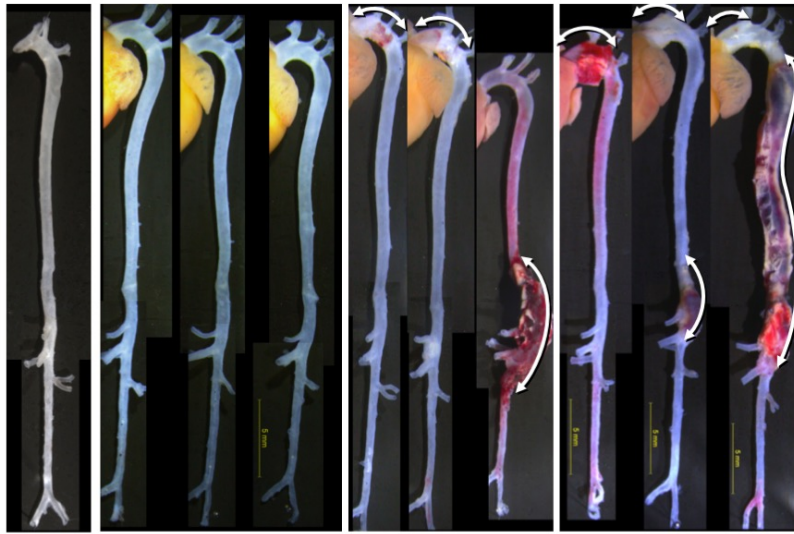
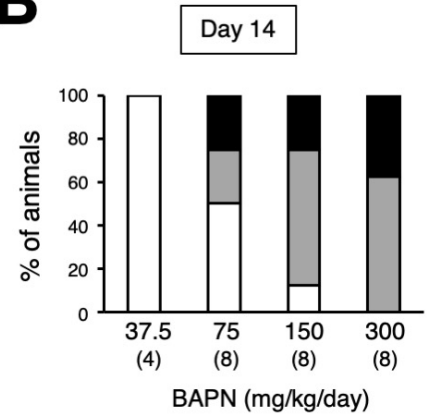
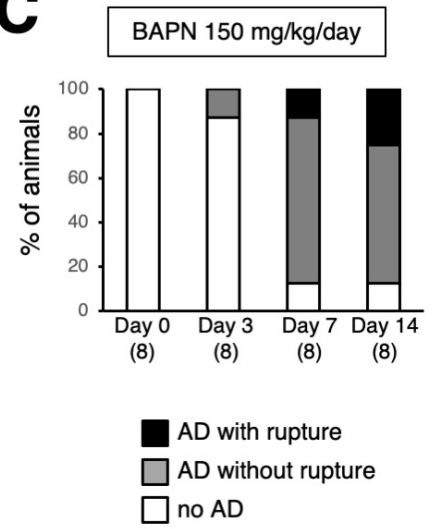
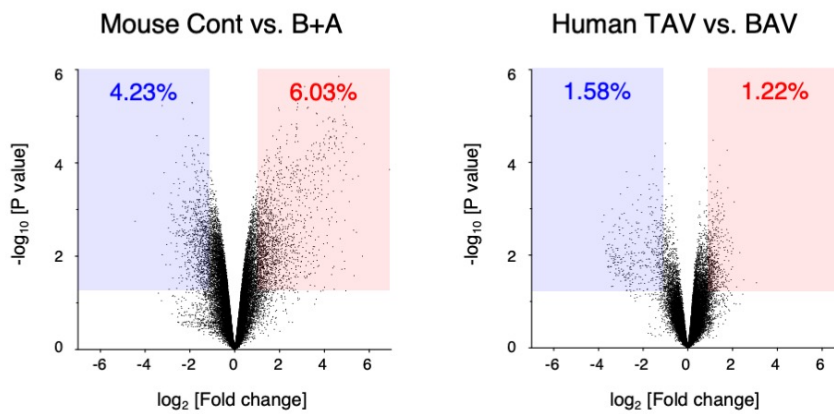
Enrichment Score: 3.67

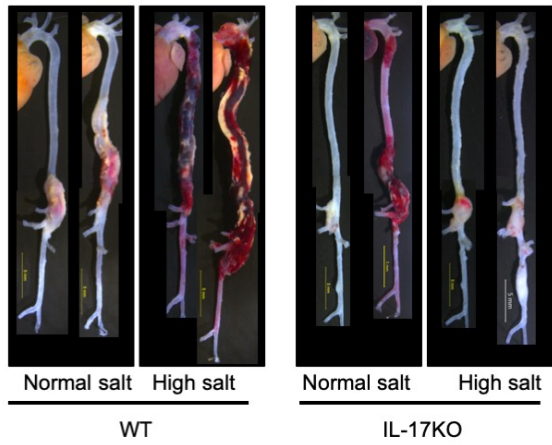
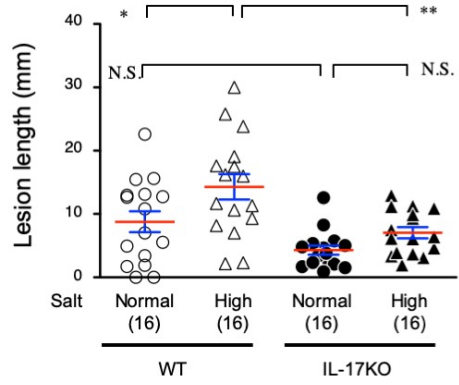
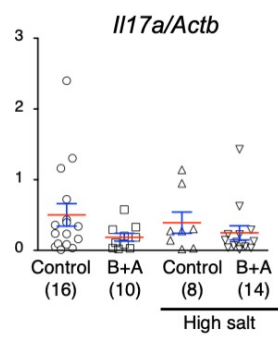
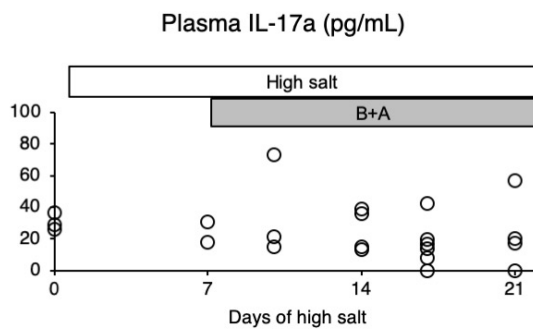
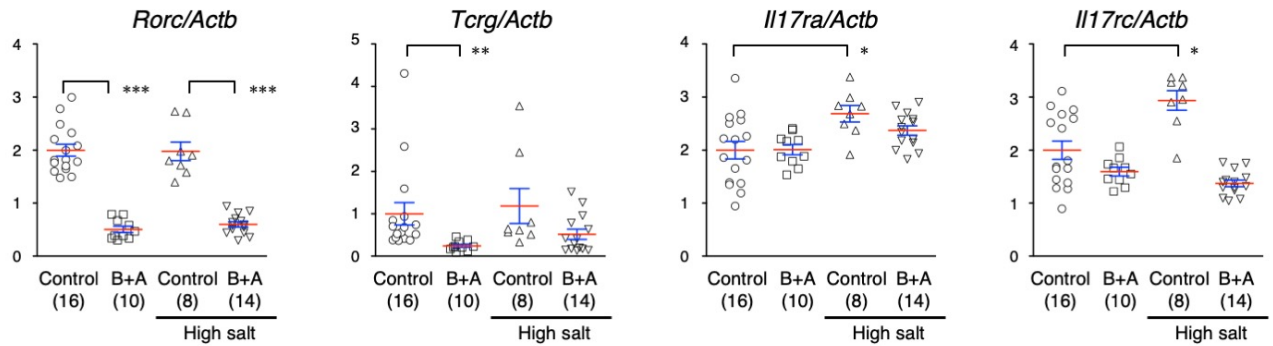
GO:0030003~cellular cation homeostasis
GO:0055080~cation homeostasis
GO:0098771~inorganic ion homeostasis

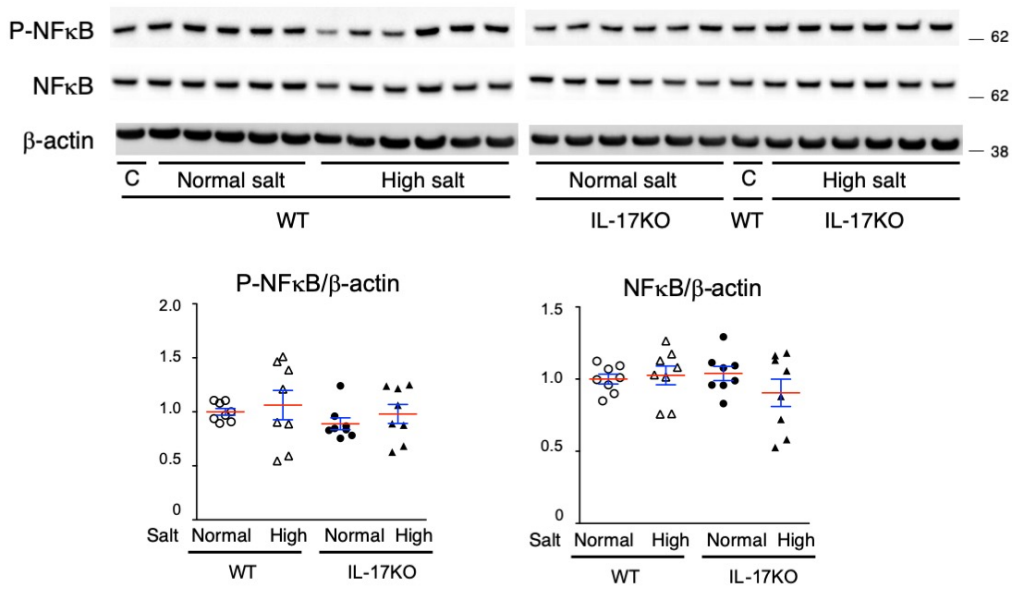
Table 3. Enrichment analysis of transcriptomes with high salt challenge and IL-17KO.

Biological process (BP)-focused gene ontology (GO) enrichment analysis was performed for the differentially expressed genes in the transcriptome of mouse aorta with high salt challenge compared to mouse aorta with normal salt (right column), and

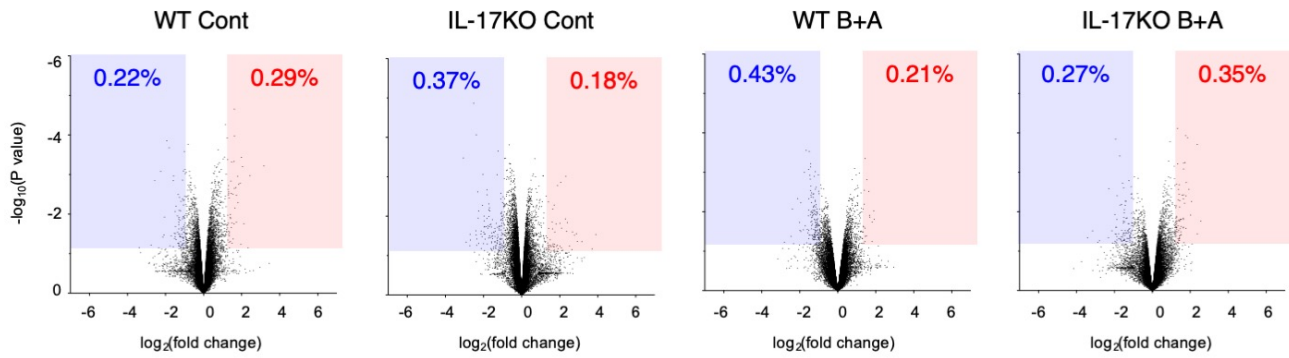
IL-17KO aorta compared to wild-type (WT) aorta. The GO terms related to tissue morphogenesis are color-coded in red.

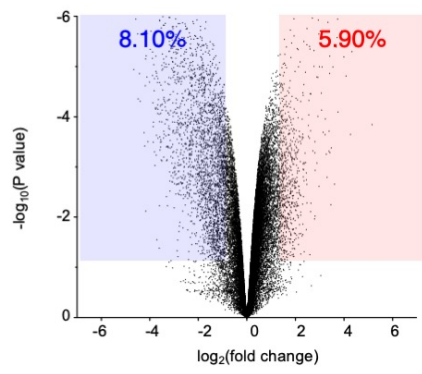
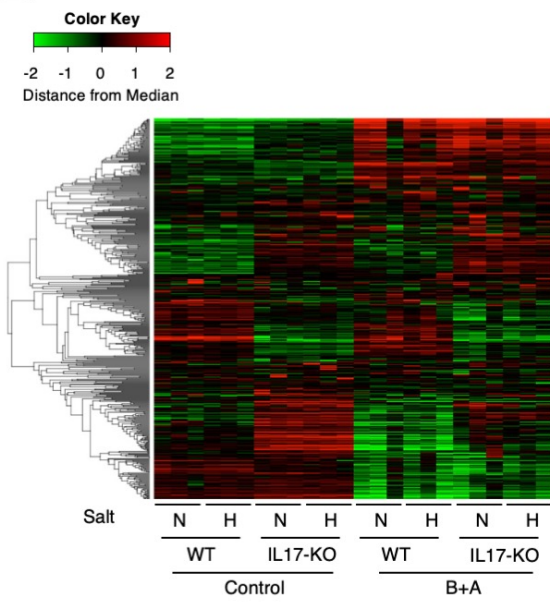
A**B****C****D**

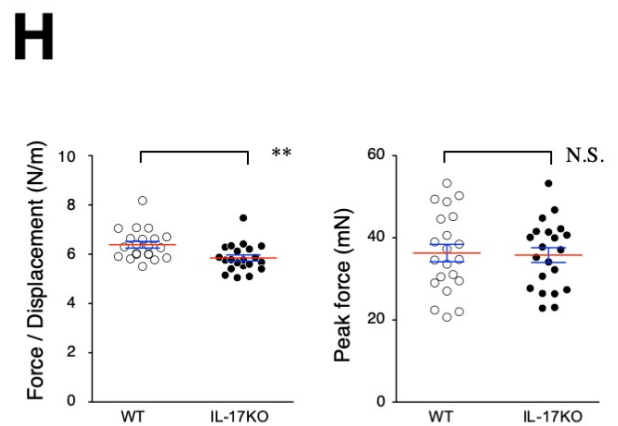
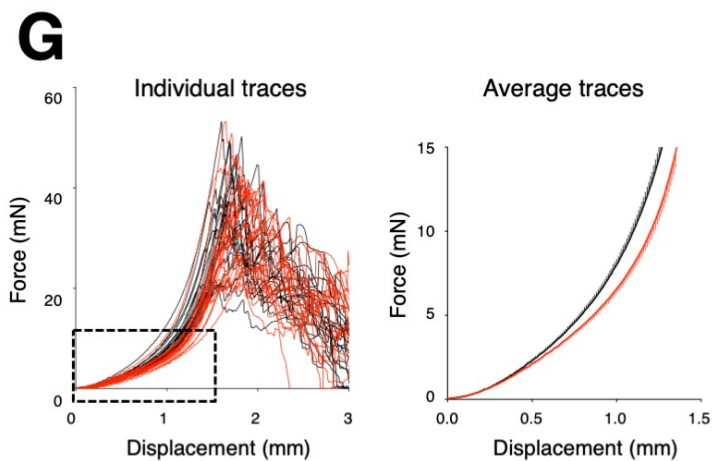
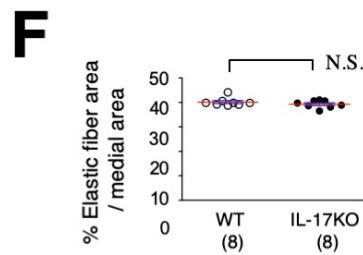
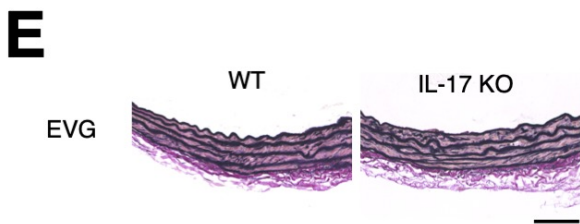
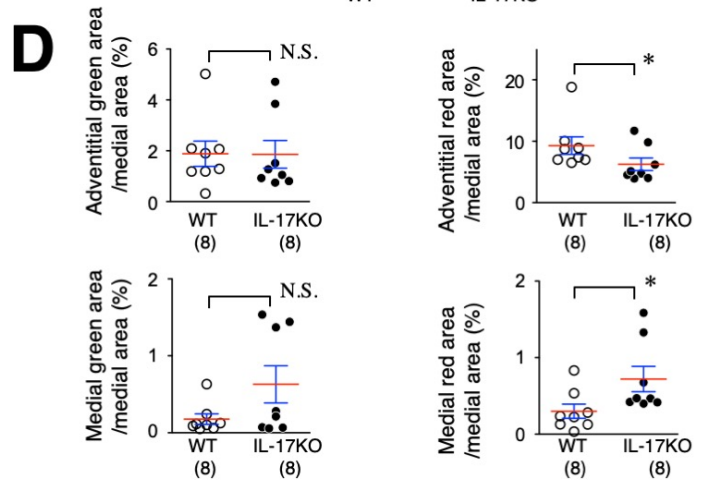
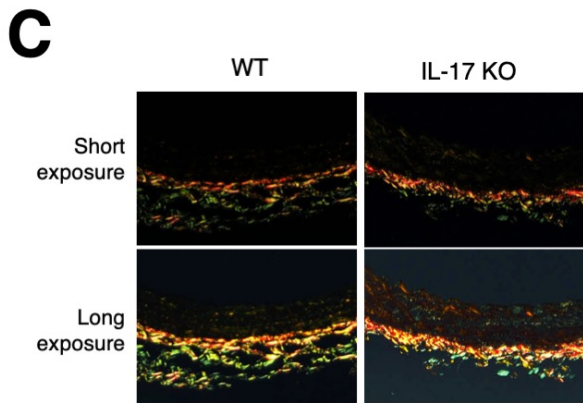
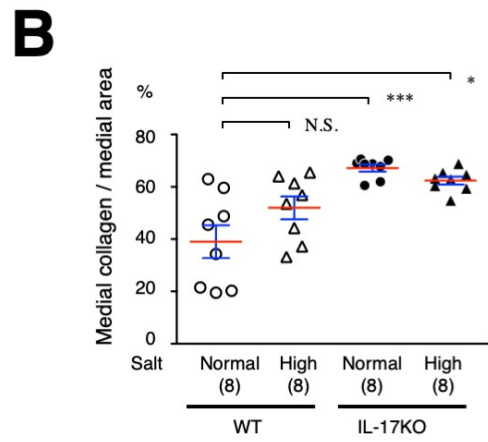
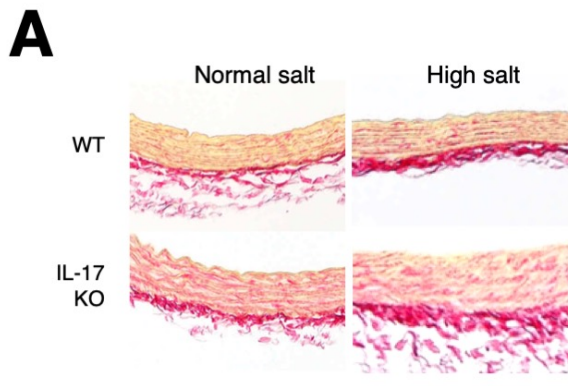
A**B****C****D**

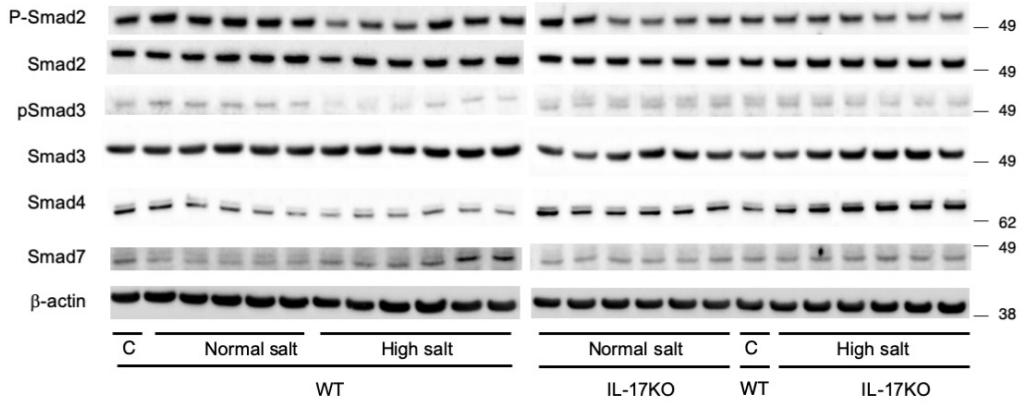
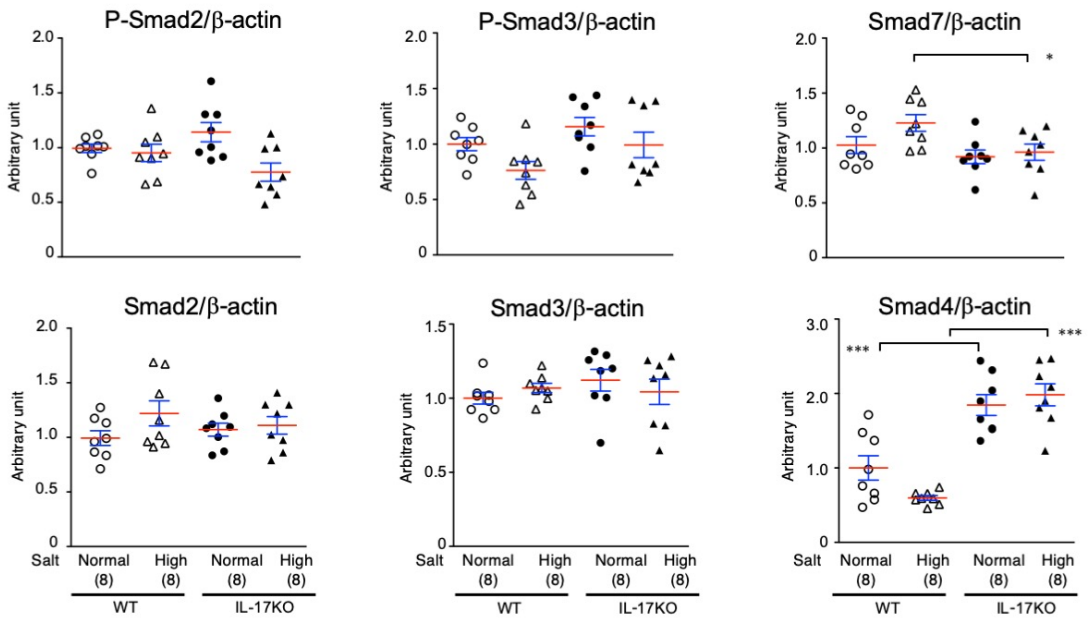
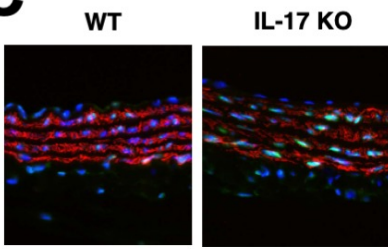
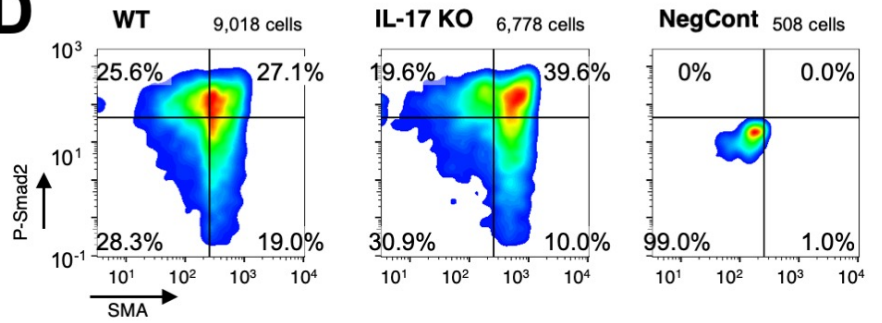
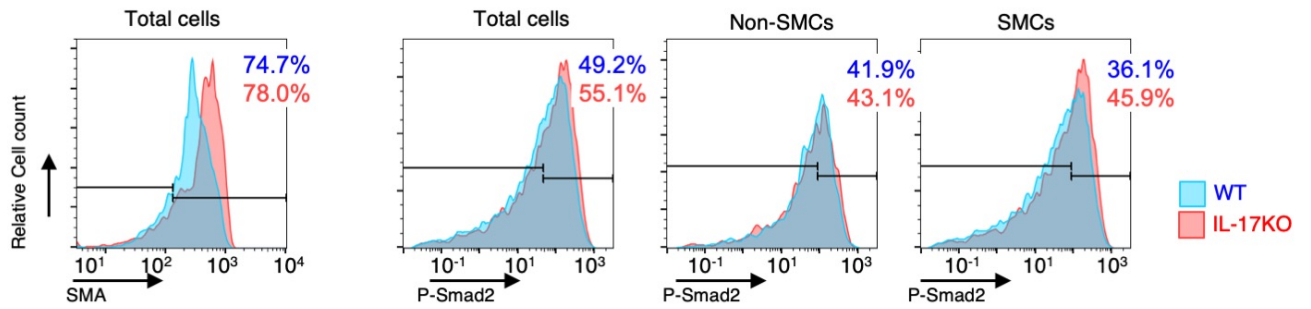
A**B**

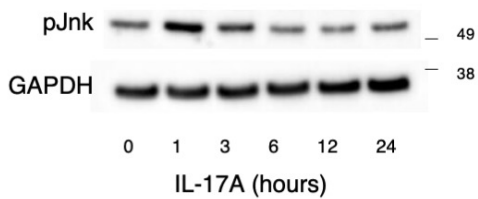
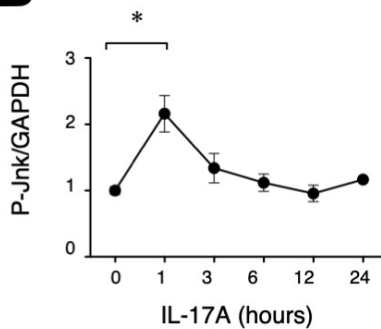
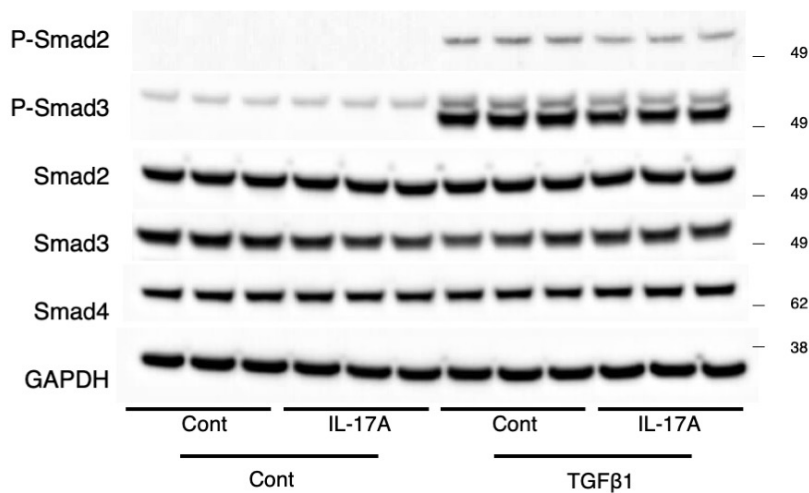
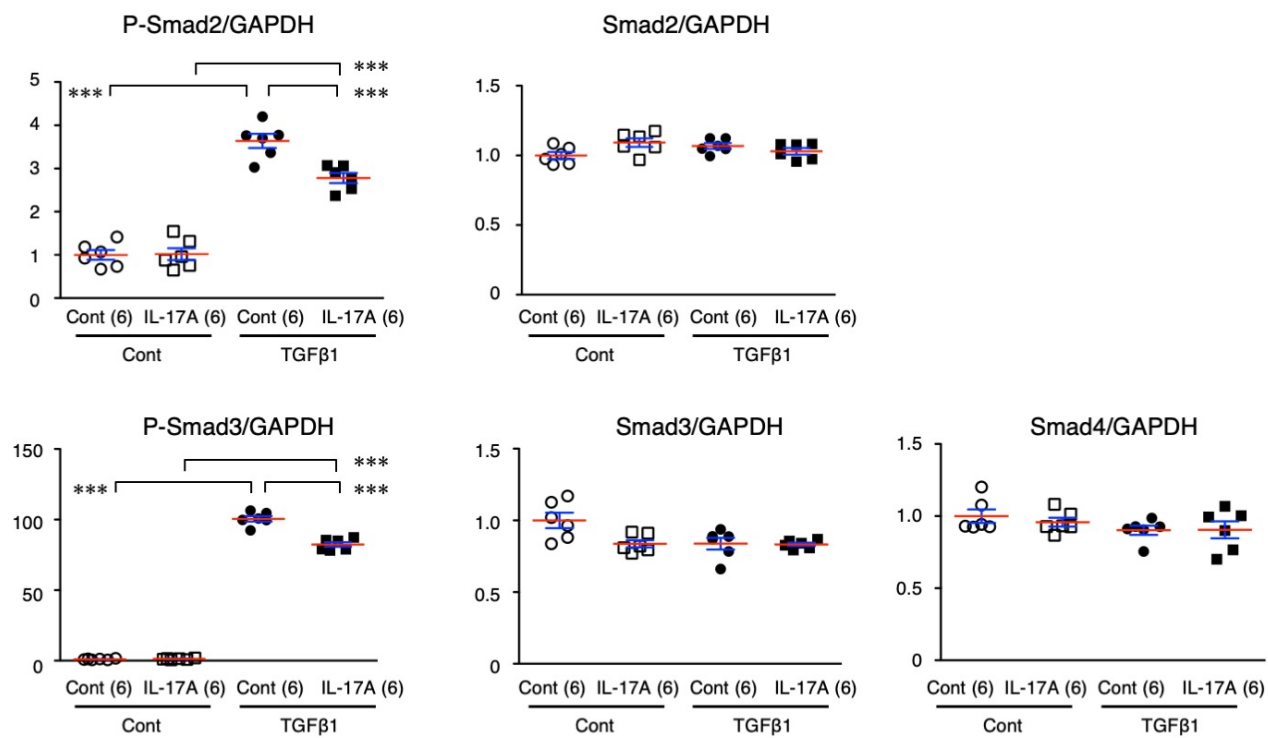
Effect of high salt

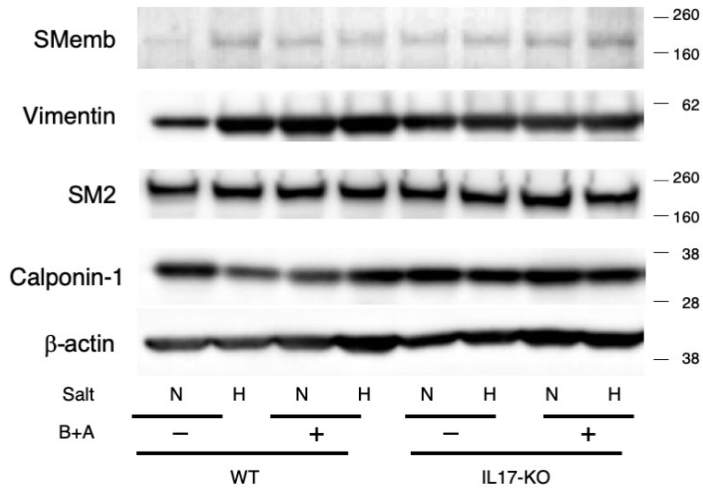
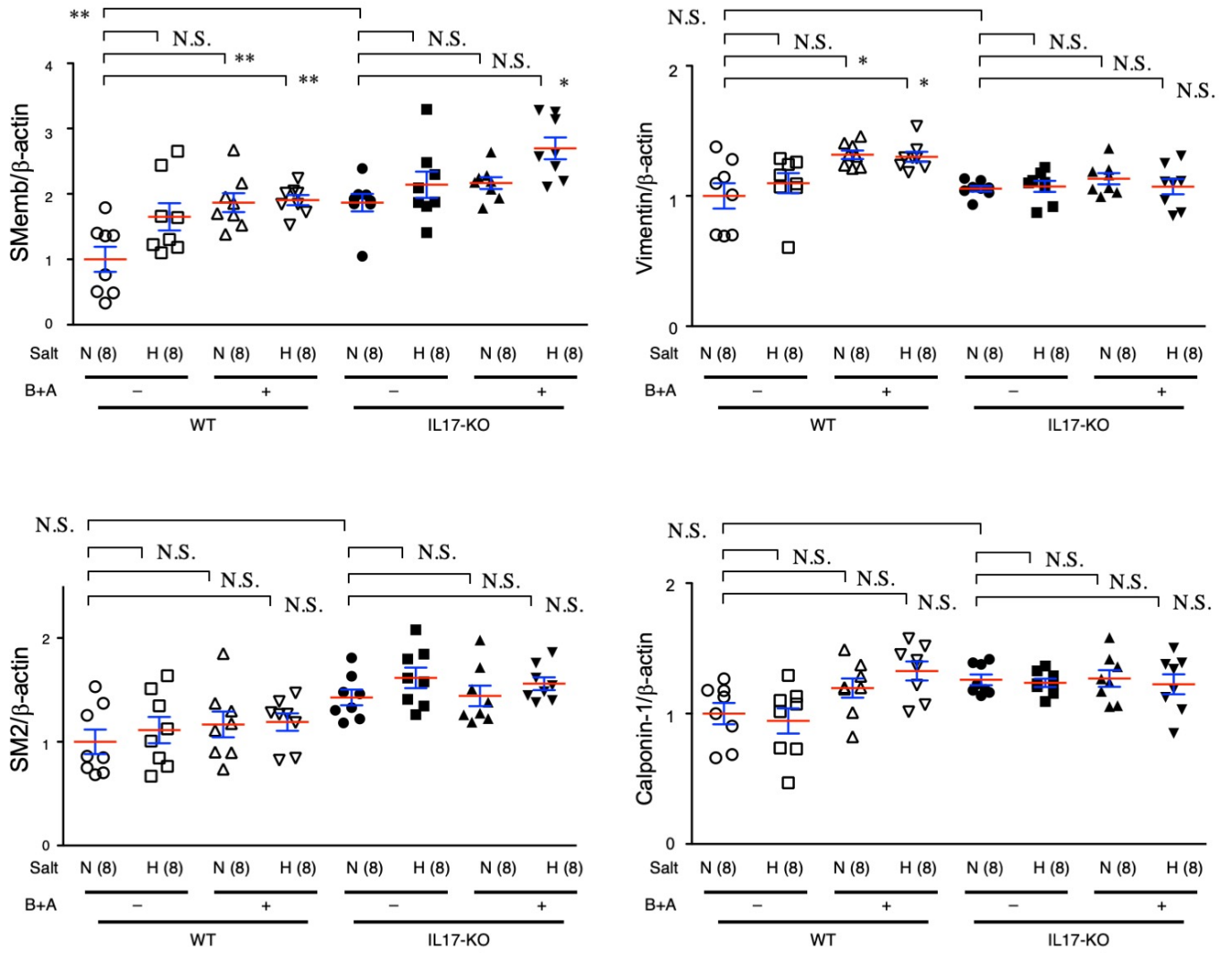


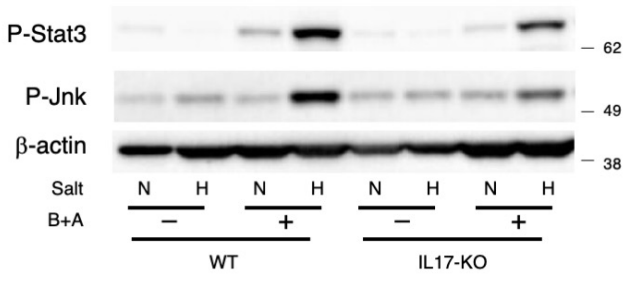
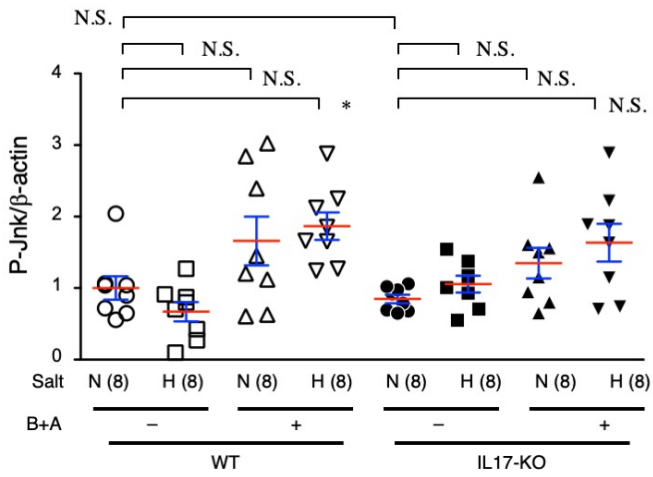
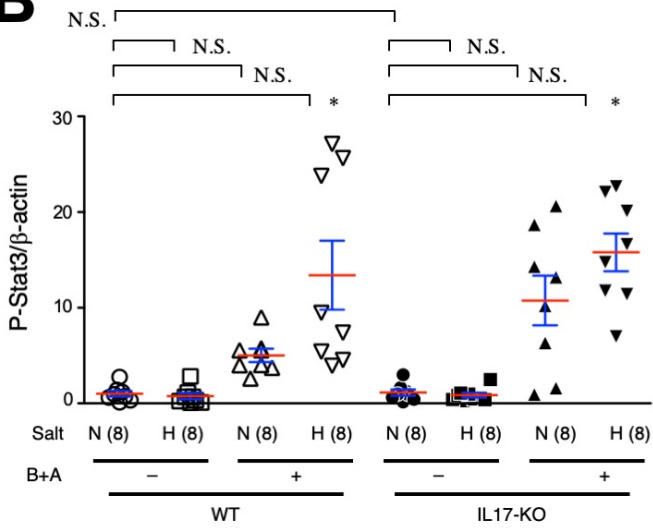
A**B**



A**B****C****D****E**

A**B****C****D**

A**B**

A**B**

SUPPLEMENTAL MATERIALS

High salt intake worsens aortic dissection in mice: involvement of IL-17A-dependent extracellular matrix metabolism

Norifumi Nishida, MD ¹, Hiroki Aoki, MD, PhD ², Satoko Ohno-Urabe, MD, PhD ¹, Michihide Nishihara, MD, PhD ¹, Aya Furusho, MD, PhD ¹, Saki Hirakata, MD ¹, Makiko Hayashi, MD ¹, Sohei Ito, MD ¹, Hiroshi Yamada, PhD ³, Yuichiro Hirata, MD, PhD ⁴, Hideo Yasukawa, MD, PhD ¹, Tsutomu Imaizumi, MD, PhD ⁵, Hiroyuki Tanaka, MD, PhD ⁴, Yoshihiro Fukumoto, MD, PhD ¹

Affiliations

1. Division of Cardiovascular Medicine, Department of Internal Medicine, Kurume University School of Medicine, Kurume, Japan
2. Cardiovascular Research Institute, Kurume University, Kurume, Japan
3. Department of Biological Functions Engineering, Graduate School of Life Science and Systems Engineering, Kyushu Institute of Technology, Kitakyushu, Japan
4. Division of Cardiovascular Surgery, Department of Surgery, Kurume University School of Medicine, Kurume, Japan
5. International University of Health and Welfare, Fukuoka, Japan

Major Resources Tables

Animals (in vivo studies)

Species	Vendor or Source	Background Strain	Sex
Mouse	Tokyo University of Science, Center for Animal Disease Models	C57BL/6J	Male

Animal breeding

	Species	Vendor or Source	Background Strain	Other Information
Parent - Male	Mouse	Tokyo University of Science, Center for Animal Disease Models	C57BL/6J	<i>117a</i> deleted
Parent Female -	Mouse	Tokyo University of Science, Center for Animal Disease Models	C57BL/6J	<i>117a</i> deleted

Antibodies

Target antigen	Vendor	Catalog #	Working concentration (µg/mL)	Applications
β-actin	Cell Signaling Technology (CST)	#4970	0.05	WB
Calponin 1	Abcam	#ab46794	0.02	WB
GAPDH	Millipore	#MAB374	0.2	WB
NFκB	CST	#8242	1	WB
P-Jnk	CST	#4671	0.9	WB
P-NFκB	Enogene	#E011260-1	1	WB
P-Smad2	CST	#3108	0.05	WB

Antibodies (cont'd)

Target antigen	Vendor	Catalog #	Working concentration (µg/mL)	Applications
P-Smad3	Abcam	#ab52903	0.25	WB
P-Stat3	CST	#9145	0.5	WB
SM2	Yamasa	#7601	1:400, ascites (antibody concentration undetermined)	WB
Smad2	CST	#5339	0.28	WB
Smad3	Abcam	#ab40854	1	WB
Smad4	Abcam	#ab195554	0.1	WB
Smad7	Abcam	#ab190987	0.5	WB
SMemb	Abcam	#ab684	1:1000, ascites (antibody concentration undetermined)	WB
Vimentin	Abcam	#ab92547	0.25	WB
Mouse IgG	Jackson ImmunoResearch	#715-165-151	7.5	IF, Cy3-conjugated donkey anti-mouse IgG antibody
pSmad2	ThermoFisher	#44-244G	2.0	IF
Rabbit IgG isotype control	Abcam	#ab172730	2.0	IF
Smooth muscle α -actin	Sigma-Aldrich	#A5228	0.2	IF
Mouse IgG2a isotype control	Sigma-Aldrich	#MABC004	0.2	IF

Cultured Cells

Name	Vendor or Source	Sex
Aortic smooth muscle cells, #JCRB0150	The National Institutes of Biomedical Innovation, Health and Nutrition (Tokyo, Japan)	Unknown

SUPPLEMENTAL FIGURES

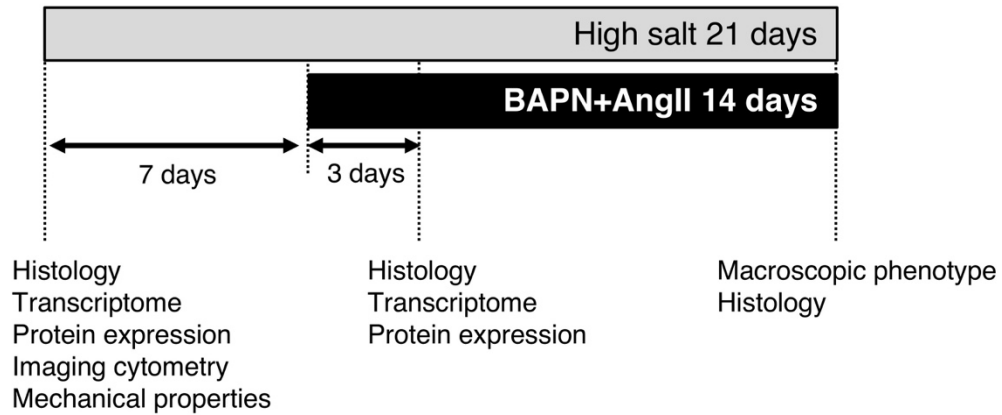


Figure I. Protocol for animal experiments.

The diagram shows the protocol for animal experiments. High salt condition (1% NaCl in drinking water) was maintained for 7 days before and throughout the AD-induction period with BAPN+AngII. Histological and expression analyses were performed 3 days after starting BAPN+AngII when visible AD was not observed. Macroscopic phenotype and histological analyses were performed at the end of 14 days of BAPN+AngII with or without high salt challenge.

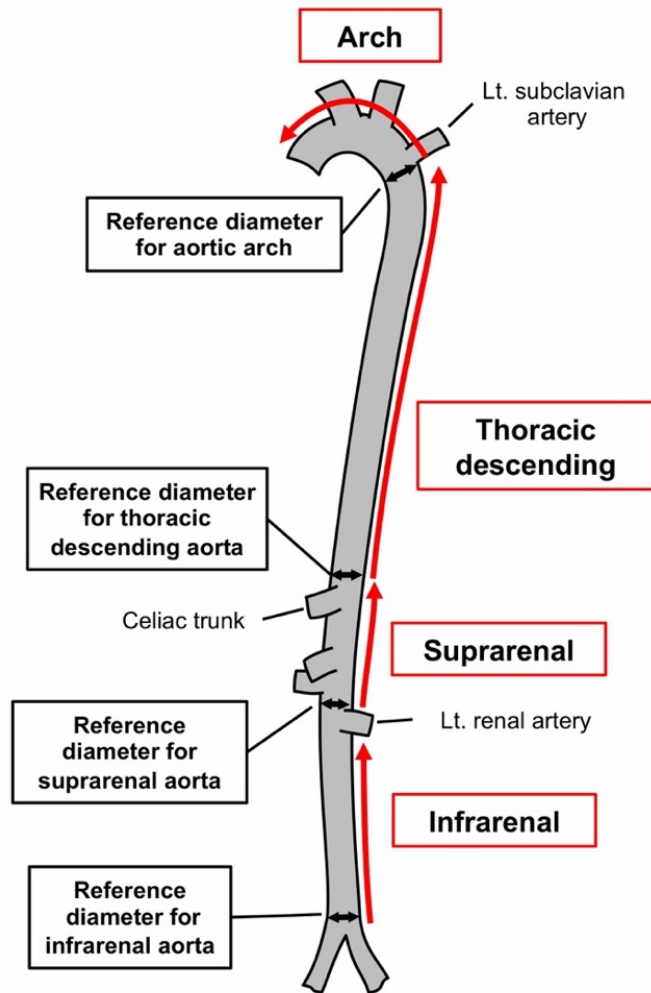


Figure II. Regional assessment of aortic wall destruction in the AD model.

The diagram shows the aortic segments (red arrows) and corresponding reference diameters at the distal site of each segment (black double arrows). The lesion length with aortic wall destruction due to AD was measured in four segments: the arch, thoracic descending, suprarenal, and infrarenal. In this study, a lesion with aortic wall destruction due to AD was defined by an at least 1.5-fold increased diameter compared to the reference diameter in each segment. The reference diameters were measured in eight mice of the relevant genotype and the mean values used.

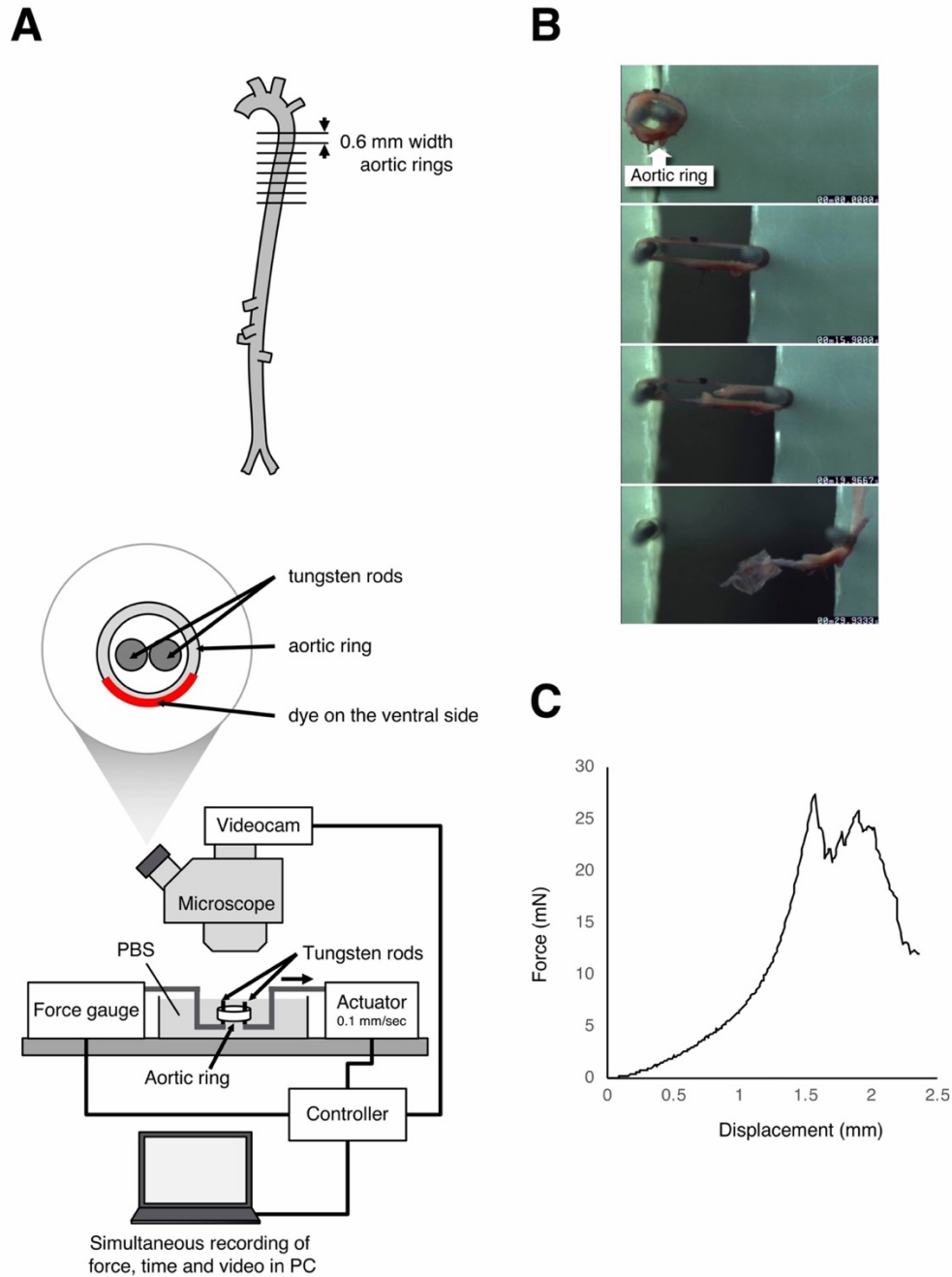


Figure III. Measurement of the biomechanical properties of the aortic wall.

(A) Diagrams of the procurement of aortic rings from the descending thoracic aorta (top) and the device for measuring the force-displacement relationship of the aortic rings (bottom). (B, C) A representative video recording (B) and force-displacement curve (C).

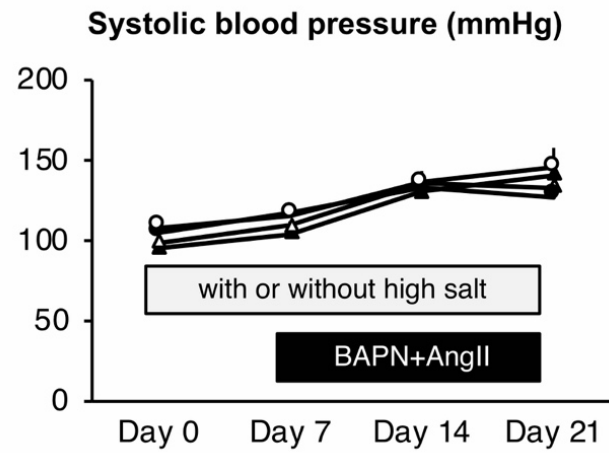
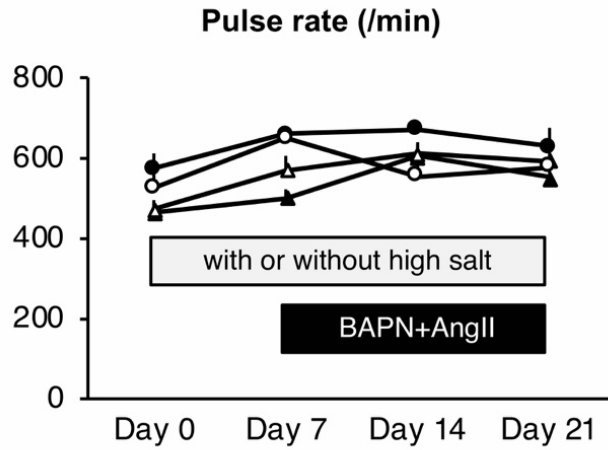


Figure IV. Hemodynamic parameters in the AD model.

Pulse rate and systolic blood pressure in the AD model with (High salt, closed symbols) or without high salt (Normal salt, open symbols) intake in wild-type (circles) and IL-17KO (triangles) mice. Data represent the mean \pm standard error for 8–12 mice in each group.

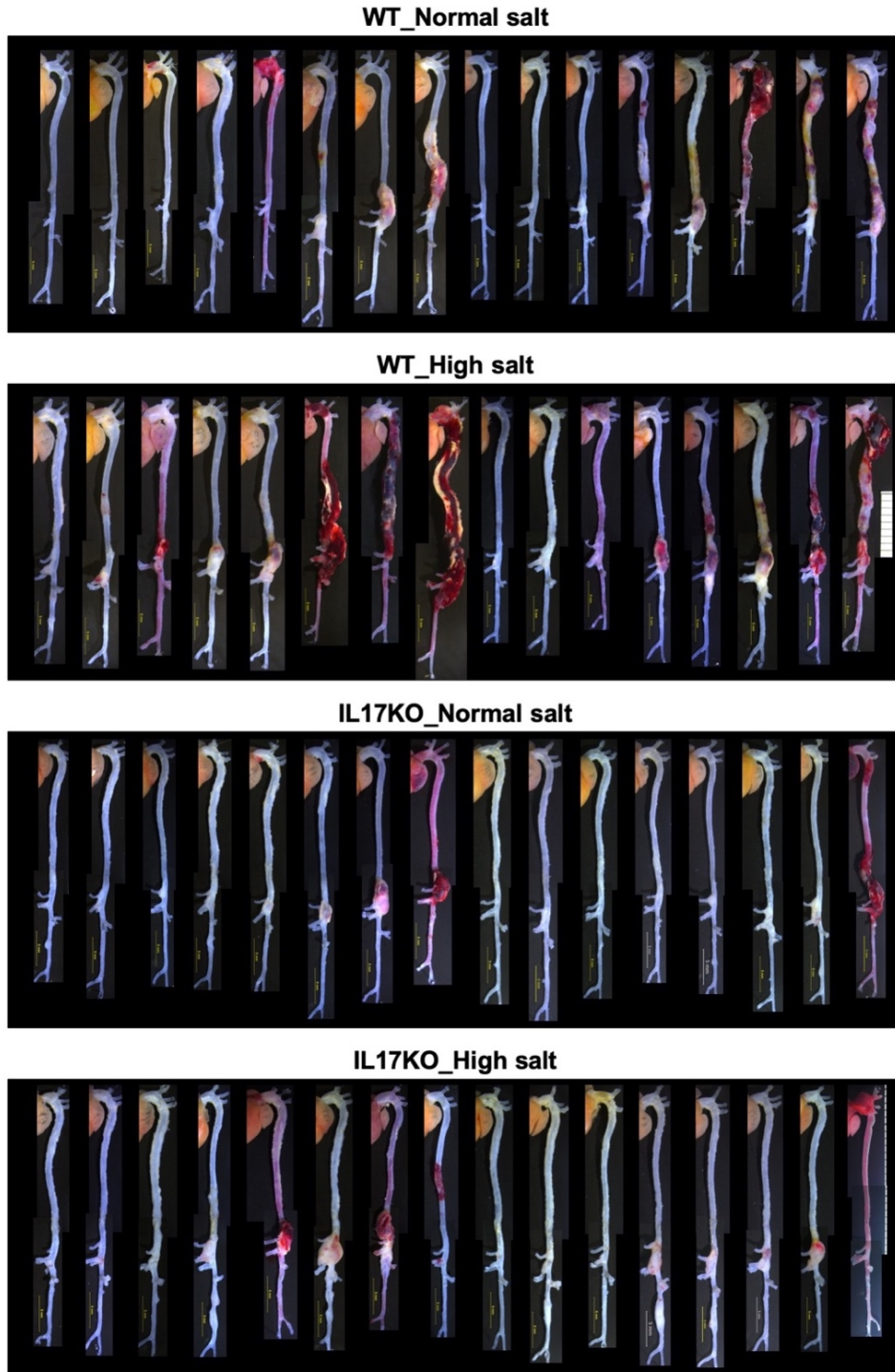


Figure V. Macroscopic images of mouse AD model.

Macroscopic images are shown for aortas of wild type (WT) and IL-17KO mice 14 days after starting BAPN+AngII infusion with (High salt) and without (Normal salt) high salt challenge.

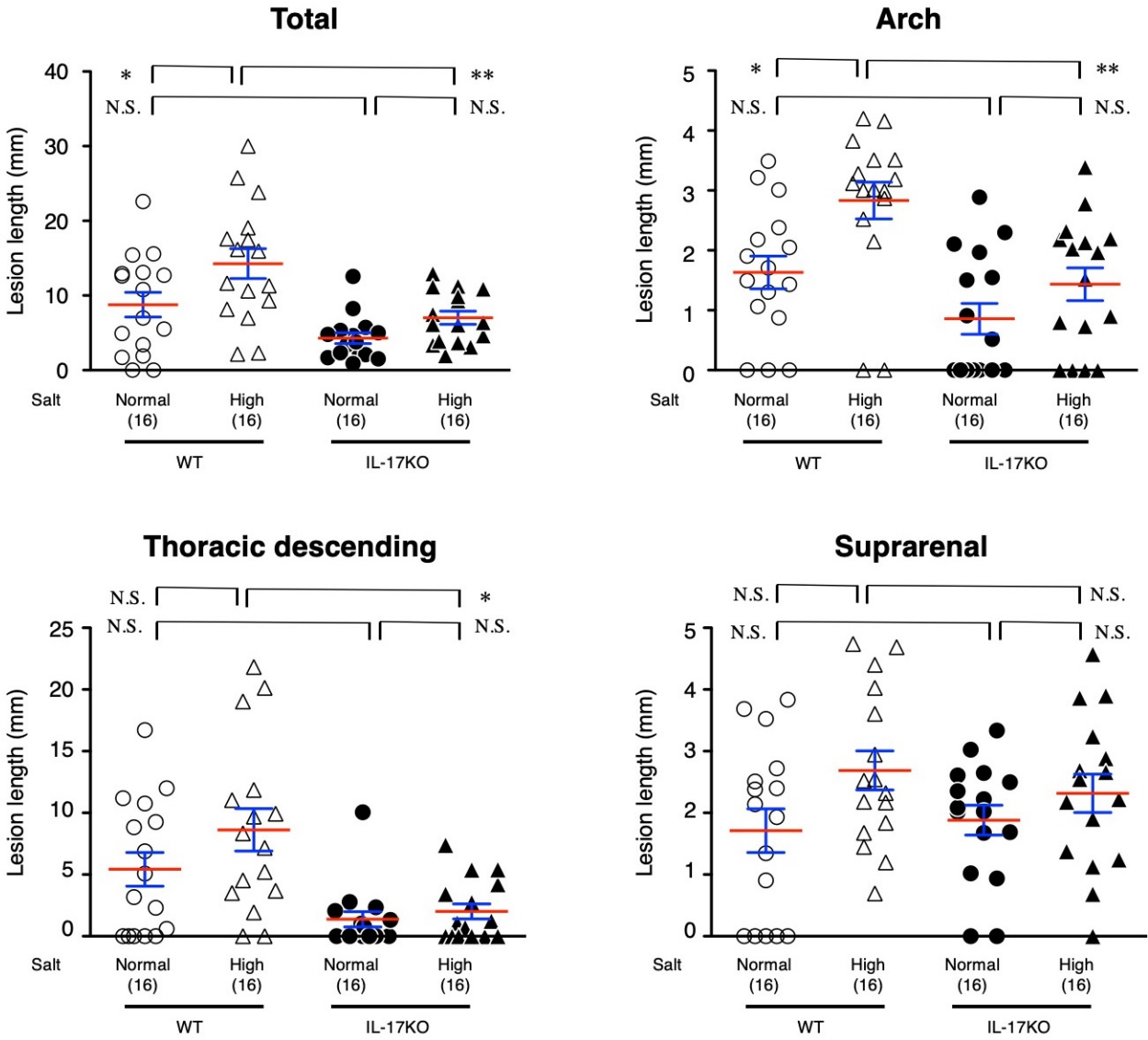


Figure VI. AD lesion length in each aortic segment and lesion scores.

The AD lesion lengths are shown for individual aortic segments. The data were obtained from the same set of experiments as shown in Figure 2B. Data are presented as the mean (red lines) \pm standard error (blue lines) of 16 mice in each experimental group; N.S., not significant, * $p < 0.05$, ** $p < 0.01$.

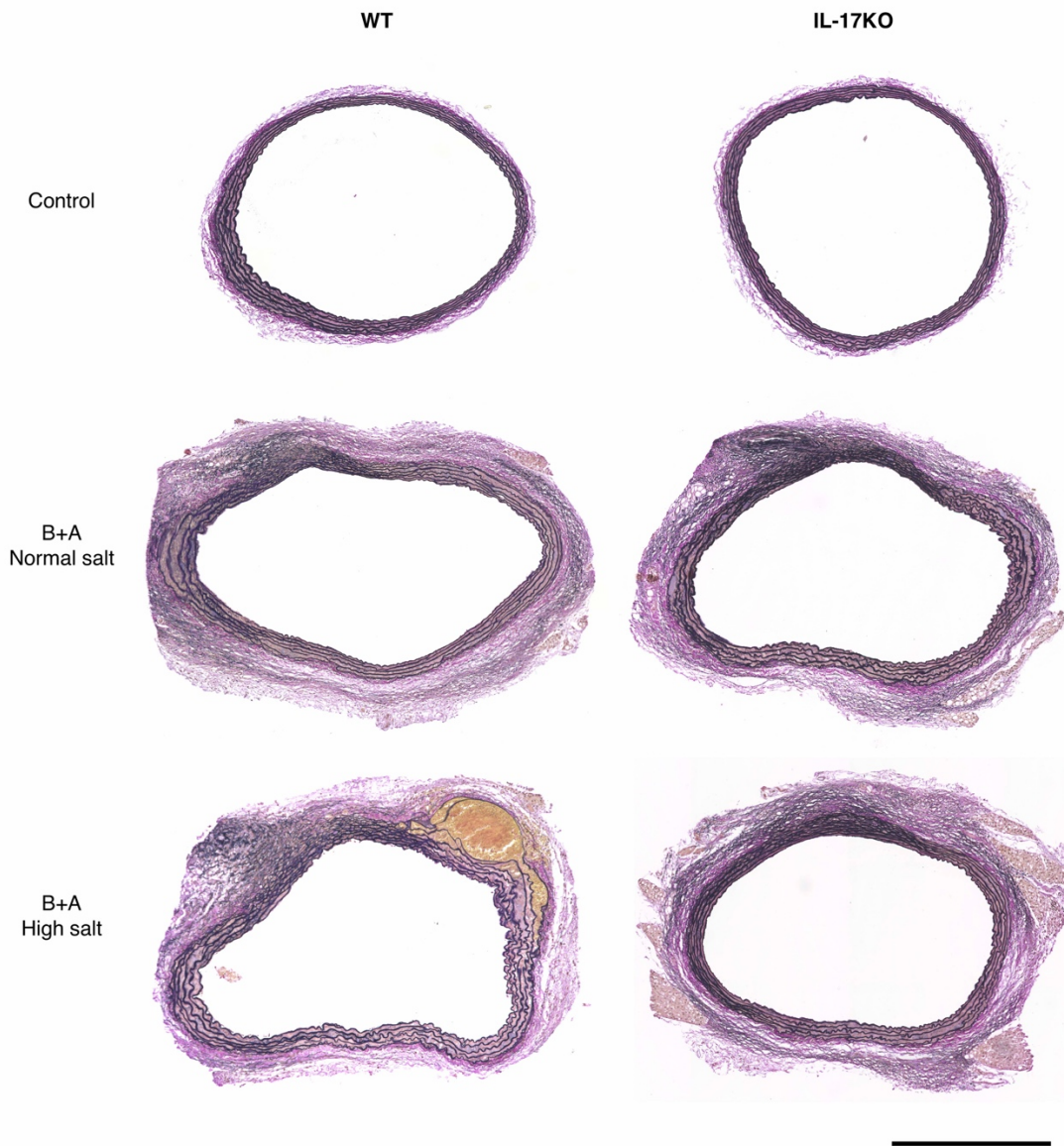
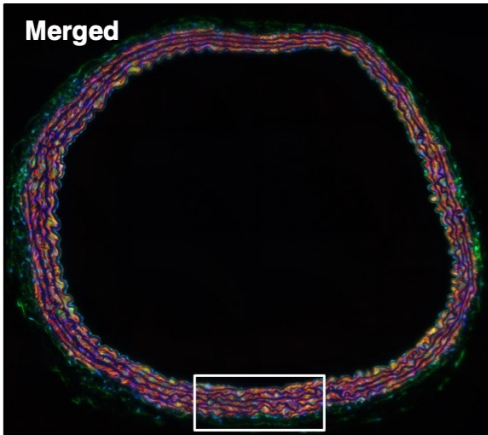


Figure VII. Histology of the AD model induced by BAPN+AngII

Representative histochemical analysis with Elastica van Gieson (EVG) stains are shown for aortic samples from WT and IL-17KO mice with or without BAPN+AngII (B+A) and high salt challenge. Scale bar = 500 μm .

P-Smad2 SMA DAPI



Rabbit IgG Mouse IgG2a DAPI

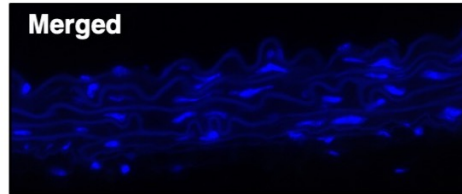
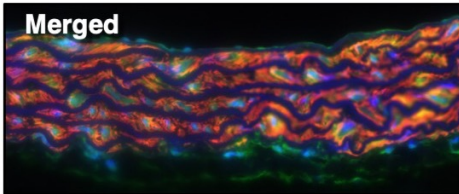
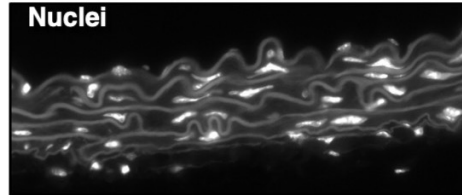
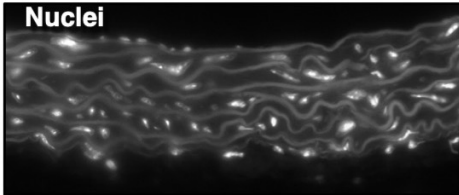
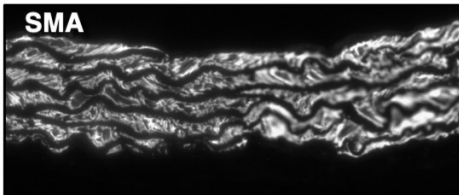
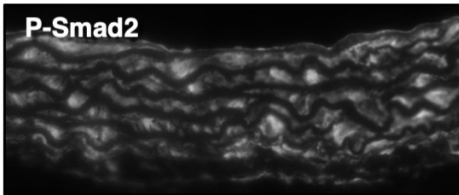
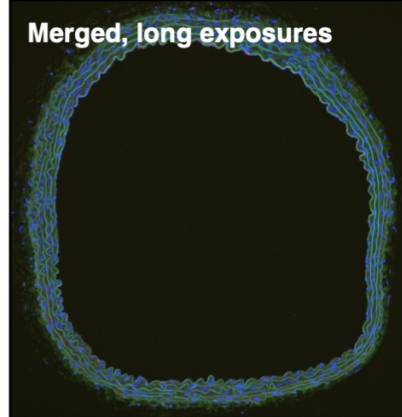
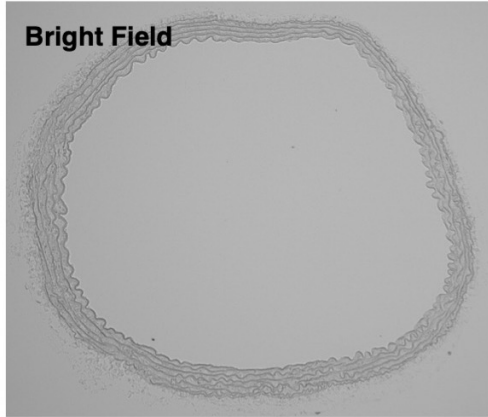
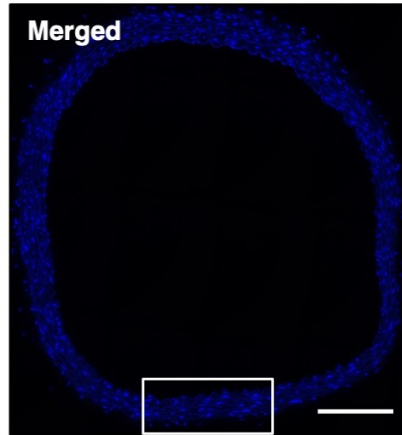


Figure VIII. Immunofluorescent staining of P-Smad2 and SMA.

Left, Representative images are shown for immunofluorescent staining of phospho-Smad2 (P-Smad2), smooth muscle α -actin (SMA), and nuclei (by DAPI) in aortas. Right, Images of the negative control in which the sample was processed with isotype control antibodies corresponding to P-Smad (rabbit IgG) and SMA (mouse IgG2a) antibodies. The bottom panels show the enlarged images for the area indicated by the rectangles in the top panels. The short exposure of the aortic tissue treated with the isotype control antibodies exhibits only DAPI fluorescence, and the long exposure image exhibits DAPI fluorescence and autofluorescence of elastic lamellae, demonstrating the specificity of P-Smad2 and SMA antibodies. Scale bar = 200 μ m.

Confocal z-series

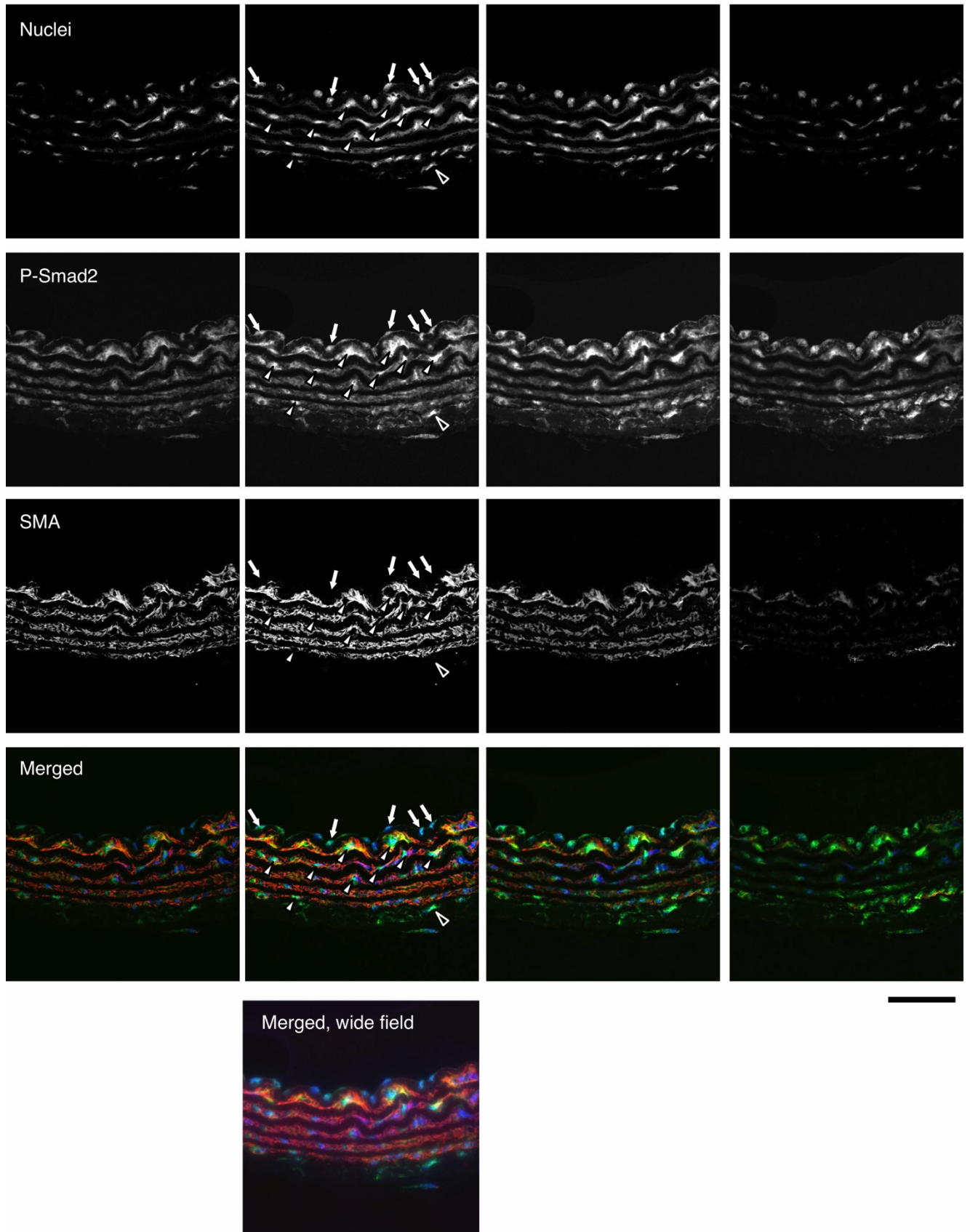


Figure IX. Confocal imaging of P-Smad2 and SMA.

Representative z-series images of optical sectioning by the laser confocal microscope for immunofluorescence staining of P-Smad2, smooth muscle α -actin (SMA), and nuclei. In merged images, nuclei, P-Smad2, and SMA are pseudo-colored blue, green, and red, respectively. White arrowheads, black arrowheads, and white arrows indicate SMA-positive cells, SMA-negative adventitial cells, and SMA-negative endothelial cells, respectively. An image from the conventional wide-field fluorescence microscope is also shown for the corresponding field. Scale bar = 50 μ m. The z-series images show that the 5- μ m sections contain a single layer of nuclei, and part of the P-Smad2-positive nuclei were surrounded by SMA, indicating that these cells were P-Smad2-positive smooth muscle cells.

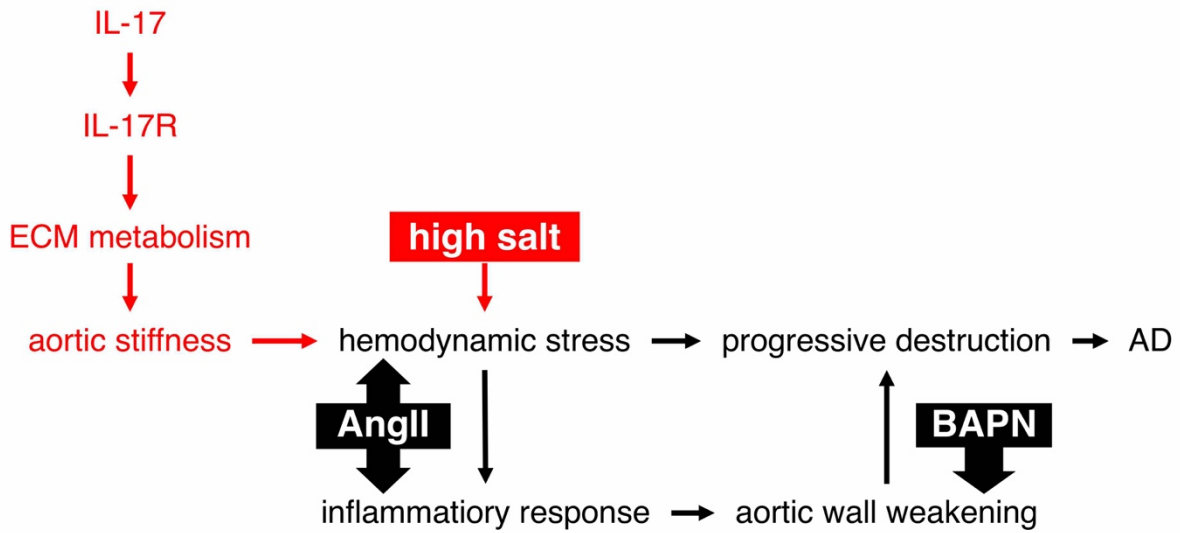


Figure X. Proposed mechanism for high salt and IL-17- dependent worsening of AD.

The AD model was created by continuous infusion of angiotensin II, which induces an inflammatory response and hemodynamic stress in aortic walls, and BAPN, which weakens aortic walls. IL-17 modulates ECM metabolism, causing aortic stiffness. High salt challenge augments the hemodynamic stress on stiff aorta, leading to a worsening of AD.

LEGENDS FOR SUPPLEMENTAL TABLES

Table I. Functional annotation of genes induced by BAPN+AngII.

Genes significantly induced by BAPN+AngII challenge (fold changes > 2.0 and $p < 0.05$) underwent functional annotation analysis using DAVID. The results correspond to the hierarchical clustering analysis and heatmap representation in Figure 1C.

Table II. Functional annotation of genes suppressed by BAPN+AngII.

Genes significantly suppressed by BAPN+AngII challenge (fold changes < 0.5 and $p < 0.05$) underwent functional annotation analysis using DAVID. The results correspond to the hierarchical clustering analysis and heatmap representation in Figure 1C.

Table III. Transcriptome of ECM-related genes.

The results of the transcriptome analysis are shown for genes with “extracellular matrix” in their Gene Ontology terms. The result corresponds to the hierarchical clustering analysis and heatmap representation in Figure 5.